PHILOSOPHICAL TRANSACTIONS OF THE ROYAL SOCIETY A MATHEMATICAL, PHYSICAL & ENGINEERING SCIENCES

The excitation of waves on a flexible panel in a uniform flow

Anthony D. Lucey

Phil. Trans. R. Soc. Lond. A 1998 **356**, 2999-3039
doi: 10.1098/rsta.1998.0306

THE ROYAL SOCIETY

The excitation of waves on a flexible panel in a uniform flow

By Anthony D. Lucey

Department of Engineering, University of Warwick, Coventry CV4 7AL, UK

Received 6 November 1995; revised 26 November 1996; accepted 21 August 1997

Contents

The wave-bearing behaviour of a finite flexible plate in a uniform flow is studied when a source of continuous oscillatory excitation is present. The method of numerical simulation is employed so that any prescription of response is avoided. A series of numerical experiments is carried out and analysed using methods similar to those applicable to a physical experiment. It is found that the plate can respond at frequencies other than that of the driver; these frequencies may either be present in the start-up procedure or be generated by wave conversions at the panel edges. At early times in the response evolution, two types of behaviour are evident. These may be separately characterized as response to low-frequency excitation and response to high-frequency excitation. The former is dominated by spatially growing waves and the latter by absolute stability. The long-time behaviour of the flexible panel shows disturbance amplitude growth at all locations for flow speeds that approach zero in the limit of an infinitely long flexible plate. For parameters corresponding to a realistic flexible panel, the long-time growth of the deformation is found to be attributable to a combination of low-frequency unstable waves which are capable of convecting wall energy and thus disturbance growth to all parts of the flexible panel; the mechanism for this features repeated wave conversions at the panel ends. This convective mechanism predominates despite the presence of an absolute instability found in the system studied here. In the later stages of the flexible-panel response, the line excitation is largely insignificant. An attempt is made to reconcile the observations of the present numerical experiments with the predictions of hydroelastic boundary-value studies of an infinitely long flexible plate and the rigorous structural-acoustics approach to the problem in which causality is a key element.

Keywords: aero/hydroelasticity; structural acoustics; numerical simulation; oscillatory excitation; finiteness effects; absolute/convective instability

PHILOSOPHICAL TRANSACTIONS OF THE ROYAL SOCIETY A MATHEMATICAL, PHYSICAL & ENGINEERING SCIENCES

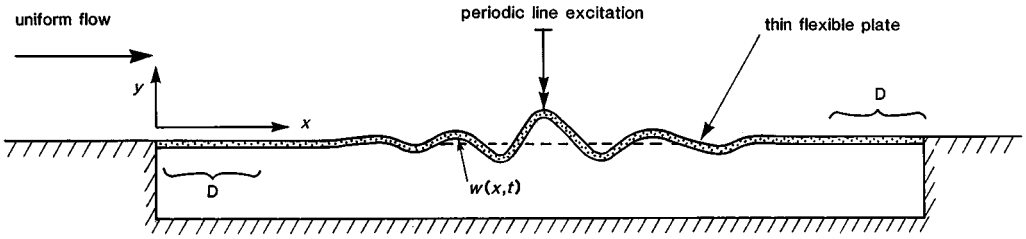

Figure 1. Schematic of the finite flexible panel and line excitation. D is the region of high damping.

1. Introduction

The interaction of a flexible panel with a fluid flow is a phenomenon which has been widely studied in aero/hydroelasticity where the problem is usually described as one of 'panel flutter'. Hitherto, the practical concern has been that, in the long-time limit, the flexible panel might experience destructive instability. However, a new focus has relatively recently been given to this problem by workers in the structural-acoustics community. In particular, Brazier-Smith & Scott (1984) and Crighton & Oswell (1991) direct interest to the question of how the presence of an adjacent fluid flow might affect the propagation of waves in the flexible wall. This subtle change of emphasis has brought to light a complex variety of waves which might exist within the simplicity of a system comprising a flexible plate interacting with a uniform flow. Moreover, by adopting the approaches of structural acoustics, both Brazier-Smith & Scott (1984) and Crighton & Oswell (1991) are able to incorporate a source of disturbance in their theoretical models—an impulse excitation in the former and continuous periodic line-excitation in the latter. This new feature begins to address the important question of how disturbances might come into being; in contrast, aero/hydroelastic stability studies are most often couched as boundary-value problems. Furthermore, the location of the disturbance source divides a flexible panel into upstream and downstream regions wherein different responses may be manifest.

The present paper brings to bear a different approach—that of numerical simulation—to study a set-up similar to that used in the Crighton & Oswell (1991) problem. However, there exists an important difference in scope between the present work and the very complete theoretical analysis of Crighton & Oswell which enables them to evaluate both the flexible-plate *and* fluid-energy densities in addition to isolating the energy fluxes associated with wave propagation in the coupled system. Such an approach permits Crighton & Oswell to identify a rich variety of waves, some of which possess very unexpected features and which may now be sought in other wave-bearing systems. In contrast, the standpoint of an experimentalist is taken in the present work. Here, the focus is placed entirely on characterizing the evolution of wave-like disturbances in the flexible plate. In engineering applications, for example, this information could be used to determine whether, and how, the amplification of such disturbances might damage or destroy a flexible panel. Nevertheless, the fluid *effects* are incorporated in the same way as in Crighton & Oswell so that any waveform existing in the flexible plate is automatically accompanied by an identical waveform in the fluid. In the present work we evaluate the energy density of the wave travelling in the flexible plate and use this to monitor the evolving deformation.

However, we are not able to evaluate the energy characteristics of the accompanying wave in the fluid. Consequently, many of the unusual features found in Crighton & Oswell (1991) may not be identified in the present study. Moreover, certain important features of our set-up, illustrated in figure 1, differ from that of Crighton & Oswell (1991); in particular, a finite flexible plate (i.e. a flexible panel) is studied here and the start-up process is included. It will also be shown that the flexible-panel ends can effectively act as wave converters, an effect identified in Crighton (1994), and thus, ultimately, the driver is not the sole source of waves. The present approach is also essentially experimental. Numerical experiments are conducted and data which could be measured in a physical experiment are collected and interpreted while maintaining an aero/hydroelastic perspective throughout; in the latter regard we are able to investigate the viability of oscillatory excitation as a means of suppressing panel instability.

Prior to discussing related work, we define the use of some terminology appearing in this paper which could otherwise be misunderstood by workers in either aero/hydroelastic or structural acoustics. The description downstream (upstream)-travelling means that the phase speed of the wave, is positive (negative). By contrast, upstream (downstream) propagation means that a spatially localized disturbance measured at the wall, being either a single wave or a wave packet, is migrating in the upstream (downstream) direction. Thus, propagation direction refers to the motion of the energy concentration of the wave; the speed of this motion is given by the magnitude of the wave's group velocity.

Hydroelastic studies of flexible-wall stability largely fall into one of two categories: the dispersion-relation approach—formulated as a force balance—of an infinitely long flexible wall (see, for example, Benjamin 1960; Dugundji *et al*. 1963; Kornecki 1978) and a Galerkin approach—formulated as an energy balance—for flexible walls of finite length (see, for example, Weaver & Unny 1971; Ellen 1973; Garrad & Carpenter 1982*b*; Lucey & Carpenter 1993*b*). In the first of these categories all disturbances are assumed to be proportional to $\exp[\mathrm{i}(kx - \omega t)]$ where k is the wavenumber and ω is the frequency. In general, both k and ω may be complex. However, in most hydroelastic studies, the investigator models, *a priori*, unstable waves as growing *either* spatially *or* temporally. In the first assumption, ω is taken to be wholly real and the spatial growth is represented by a negative imaginary part to k, while in the second assumption k is wholly real and the wave is amplified at all spatial locations through the positive imaginary part to the complex frequency. It has become common to associate the spatial approach with convective instability. In contrast, the temporal approach is not used exclusively for truly temporally growing, or absolute, instabilities. More often than not, following the example of early hydrodynamic stability theory, it is used as an approximate model for convective instabilities. Absolute and convective instabilities can only be correctly identified by allowing both k and ω to be complex and solving a proper initial-value problem where a source of disturbance originating at a finite time and location is present. This is the path adopted by Brazier-Smith & Scott (1984) and Crighton & Oswell (1991) in the context of the present problem. The essential differences between convective and absolute instabilities in fluid mechanics are presented in Gaster (1968) and Huerre & Monkewitz (1985, 1990). The application of these ideas to wall–flow interaction was initially addressed by Brazier-Smith & Scott (1984) and is also discussed in Carpenter (1990). The physical importance of this difference in a spatially homogeneous infinite domain

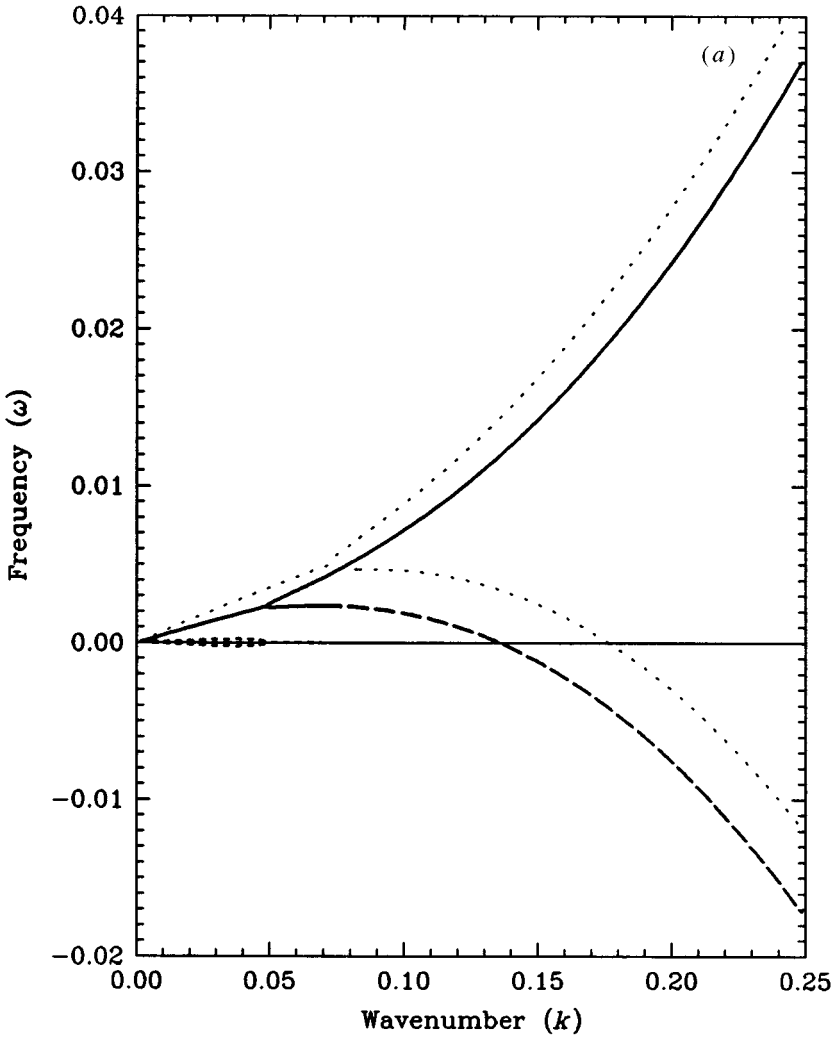

Figure 2. Dispersion diagrams. (a) Overall characteristics for two flow speeds, $U' = 0.05$ and 0.0742. ——, ω_{R} downstream at $U' = 0.05$; – – –, ω_{R} upstream at $U' = 0.05$; - - - -, ω_{I} at $U' = 0.05$; · · · ·, ω_{R} at $U' = 0.0742$.

is that, in the long-time limit, a convective instability produces no amplification of a disturbance at any fixed spatial location whereas an absolute instability would generate exponential growth at the same location.

Returning to the hydroelastic approach to the study of an infinitely long flexible wall, the wall–flow system is easily solved when unsteady potential flow is assumed, disturbances take the form $\exp[\mathrm{i}(kx - \omega t)]$ and just a single wave is considered. For the case of an infinitely long flexible plate, the dispersive characteristics $[D(k, \omega) = 0]$ are charted in figure 2a, b. For large wavenumbers, the system behaves qualitatively as in the zero-flow limit: neutrally stable waves propagate upstream and downstream. Where there is strong flexible-plate–flow coupling at the lower wavenumbers, the upstream-travelling wave changes direction and finally coalesces with the

PHILOSOPHICAL TRANSACTIONS OF THE ROYAL SOCIETY A MATHEMATICAL, PHYSICAL & ENGINEERING SCIENCES

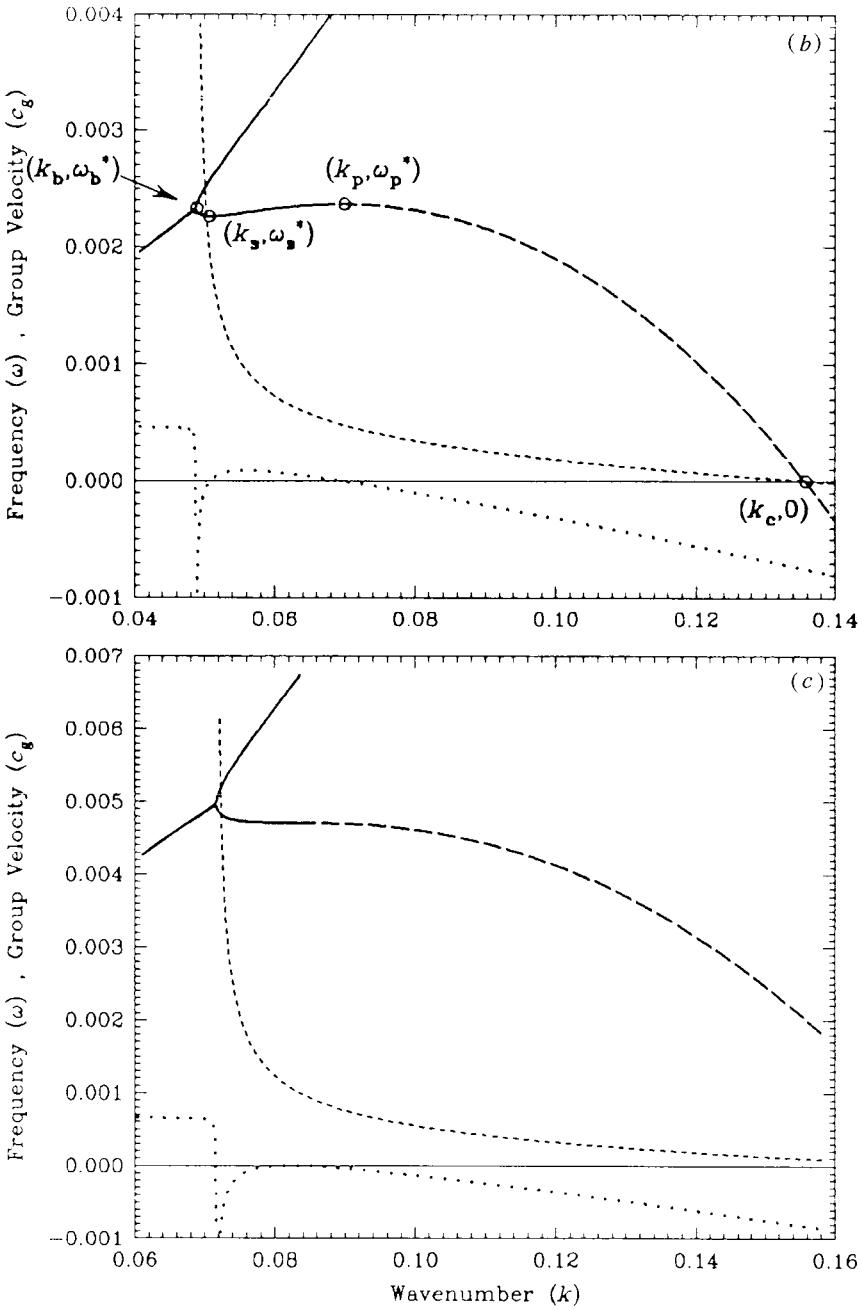

Figure 2. *Cont.* Detail and group velocity, c_g, for (*b*) $U' = 0.05$; (*c*) $U' = 0.0742$. ——, ω_R downstream; – – –, ω_R upstream; - - - -, $\omega_I \times 1000$ lower branch; · · · ·, $c_g \times 0.01$, lower branch.

downstream-travelling wave to yield a complex conjugate pair of roots. For the range of wavenumbers between k_b at the point of coalescence and k_c where the lower branch crosses the wavenumber axis, the introduction of flexible-plate damping—regardless of how little—generates a positive imaginary part to ω for the lower-branch solu-

tions. This suggests that waves in this range are unstable. The wave exactly at k_c is static; an equilibrium exists between the hydrodynamic force and the restorative force in the flexible plate due to its bending. Divergence instability occurs when the combination of wavenumber and flow speed is such that the flexible-plate deflection generates a hydrodynamic force which exceeds the accompanying restorative structural force. The resulting amplification of the wave yields an increased difference between these competing forces and continued growth ensues. Here, at a fixed flow speed, a wave in the range $k_b < k < k_c$, would satisfy this criterion, if it were static, because the hydrodynamic and plate-bending force densities are respectively proportional to the second and fourth derivatives of the deflection. However, in the absence of damping, the positive phase speed, $c = \mathrm{Re}(\omega)/k$, of any wave in this range is such that the effective flow speed, $(U_\infty - c)$, experienced by the same wave held static in a frame of reference moving at speed c, continues to yield a hydrodynamic force which exactly balances the restorative force in the flexible plate and so ensures neutral stability. Landahl (1962) explained that flexible-plate damping served to reduce the wave phase speed marginally, causing the hydrodynamic force to overcome the restorative force in the flexible plate, and thereby give rise to divergence instability. The term 'static divergence' is often used by aero/hydroelasticians to describe this instability because the critical point is at zero frequency; near the critical point, growth of divergence is predicted as a low-frequency downstream-travelling wave. The role of energy dissipation in divergence instability of an infinite flexible wall led to its being classified as class A in the scheme of Benjamin (1963) and Landahl (1962). (In the scheme used by Briggs (1964) and Cairns (1979) a class A wave corresponds to a negative energy wave (NEW).) The modal-coalescence flutter instability is described as class C, being of the Kelvin–Helmholtz type, while the conventional modified flexural waves seen at high wavenumbers are class B (or positive energy waves (PEWs)).

Hydroelastic studies of flexible walls of finite length use as their starting point a disturbance form proportional to $\exp(-\mathrm{i}\omega t)$ with the spatial dependence, or mode shape, being decomposed into a collection of orthogonal modes which satisfy the leading- and trailing-edge conditions. In marked contrast to the dispersion-relation approach, the growth in divergence instability is predicted to occur as the amplification of a standing-wave deflection and flexible-wall damping is not needed for its realization. However, by finding asymptotic expressions for the integrals of generalized hydrodynamic forces, Carpenter & Garrad (1986) have extended the methods used for finite flexible walls to study the limiting case of an infinitely long flexible wall. They showed exact agreement with the dispersion-relation predictions of critical values for the divergence-onset flow speed and wavenumber when the flexible wall possesses more than one structural component. For a simple infinite flexible wall in the form of an unsupported flexible plate this critical flow speed would be zero with the critical wavelength being infinite. However, for the case of the finite flexible plate, i.e. panel, depicted in figure 1, the critical flow speed depends upon the flexible-panel length because it is the fundamental mode which is first destabilized by divergence as the flow speed is increased. The analyses of finite flexible walls therefore strongly suggest that the divergence instability (which can be associated with the lower branch of dispersion curve for $\mathrm{Re}(\omega) > 0$ in figure 2), is class C (i.e. neither a NEW nor a PEW) because the instability is predicted to be an amplifying standing wave and flexible-wall damping is not a *sine qua non* for its existence.

The crucial differences of instability form (static deformation or travelling wave) and the role of flexible-wall damping in the predictions of the two approaches described above have in some measure been resolved by the numerical simulations of Lucey & Carpenter (1992*a*). These yield onset flow speeds and critical wavenumbers that find appropriate agreement with both of the analytical approaches. Close to, but above the onset flow speed, they show that the instability manifests itself as a slow downstream-travelling wave which, despite its downstream travel, shows growth at all flexible-wall locations. Furthermore, damping is not required for its realization. These features strongly indicate that it is an absolute instability†. Further support for this assertion is found in the very recent work of Yeo *et al*. (1996), who identify the 'pinch point' associated with the divergence eigenmode on a compliant wall with a boundary-layer flow. Experimental studies of divergence by Gad-el-Hak *et al*. (1984), albeit on a different type of flexible (or 'compliant') wall, also indicate an absolute instability. The differences between the studies of infinite and finite flexible walls are discussed by Lucey & Carpenter (1993*a*) who present a heuristic argument to show that the condition of finiteness plays a role similar to the destabilizing effect of damping in the hydroelastic stability of an infinite flexible wall. Landahl (1962) explained that the effect of damping would produce the marginal reduction of wave phase speed responsible for destabilizing the lower branch of figure 2*a*, *b* in the range $k_{\mathrm{b}} < k < k_{\mathrm{c}}$. For an undamped finite flexible wall, Lucey & Carpenter (1993*a*) argue that it is the constraint of zero motion at the ends of the flexible wall, irrespective of its length, which provides the marginal reduction to the wave phase speed, thereby causing the growth of divergence waves. Lucey & Carpenter (1993*a*) also showed that finiteness generates locally non-conservative hydrodynamic forces in the flexible-wall–flow system. In contrast, modelling an infinitely long elastic plate with a potential flow yields a fully conservative system. These considerations suggest that the analysis of an infinite flexible plate should incorporate the effects of some flexible-plate damping. In a hydroelastic-instability analysis, this would render unstable the whole of the lower branch of the dispersion curve in figure 2*a* for the wavenumber range in which $\mathrm{Re}(\omega) > 0$. If the instability existing in this region were not able to convect away, disturbance growth may dominate the response even when oscillatory excitation is present. However, what such hydroelastic studies are unable to predict is which unstable wave(s) would ultimately dominate the response.

Workers in structural acoustics (most notably Brazier-Smith & Scott (1984), Crighton (1989), Crighton & Oswell (1991) and Abrahams & Wickham (1994)) include a line disturbance source in their model problem. This is the most significant difference between their approach and those described above. In all of the studies cited immediately above, an infinitely long flexible plate is assumed. The governing equations and interfacial boundary conditions can then be transformed and solved algebraically for the Fourier transform of the wall displacement. The inversion of the transform necessitates invoking causality to identify the valid poles obtaining from a pair of quintic dispersion relations, one appropriate to locations upstream and the other to locations downstream of the driver. The linear response can then be written as a superposition of the valid contributions for each half (upstream and downstream of the driver), of the flexible wall. Furthermore, when correctly formulated, this approach rigorously determines whether an instability is convective or absolute.

† And class C in the scheme of Benjamin (1963) and Landahl (1962) (thus neither a PEW nor a NEW).

Brazier-Smith & Scott (1984) applied a line impulse excitation to initiate disturbances and charted the overall stability of the system. Above a certain flow speed, absolute instability was found in the system. A dispersion diagram at this critical flow speed is shown in figure 2*a*, *c*. Comparison with the subcritical result of figure 2*b*, shows that this instability comes about through a coalescence of the lower branch segments $[k_\mathrm{b}, k_\mathrm{s}]$ and $[k_\mathrm{p}, k_\mathrm{c}]$; the segment $[k_\mathrm{s}, k_\mathrm{p}]$ disappears in the process of increasing the flow speed. Alternatively, for the corresponding frequency range, $[\omega_\mathrm{s}^*, \omega_\mathrm{b}^*]$, where four wavenumber solutions were seen in figure 2*b*, only two wavenumber solutions are seen in figure 2*c*. It is necessary to remark here that the real frequencies, ω_b^*, ω_s^* and ω_p^* labelled in figure 2*b* show a very small numerical difference from their counterparts ω_b, ω_s and ω_p in the work of Brazier-Smith & Scott (1984) and Crighton & Oswell (1991). This is because the inclusion of flexible-plate damping when evaluating figure 2 makes all wave frequencies in the (k, ω)-plane complex. In this paper we will continue to use $\omega_\mathrm{p}^* = \mathrm{Re}\{\omega(k_\mathrm{p})\}$ to distinguish it from the wholly real value $\omega_\mathrm{p} = \omega(k_\mathrm{p})$ at the pinch point in Brazier-Smith & Scott (1984) and Crighton & Oswell (1991). Below Brazier-Smith & Scott's critical flow speed, three regions are discerned which may be categorized by frequency intervals. In the interval $[0, \omega_\mathrm{s}]$, convective instability is predicted; this can be associated with the modal coalescence seen in each part of figure 2. In the range $[\omega_\mathrm{s}, \omega_\mathrm{p}]$, the resulting wave properties are found to possess anomalous features; these can be associated with the lower branch segment $[k_\mathrm{s}, k_\mathrm{p}]$. At higher frequencies, $\omega > \omega_\mathrm{p}$, (neutrally) stable waves are predicted; these are conventional modified flexural waves as are the upstream-travelling waves with $\omega < 0$ on the lower branch in figure 2*a*, *b*.

Following the basic approach used by Brazier-Smith & Scott (1984), Crighton & Oswell (1991) conducted a comprehensive investigation of the system when the flexible plate experiences continuous oscillatory line excitation. In their paper the critical flow-speed value for the onset of absolute instability is first determined exactly. Thereafter, attention is given to the subcritical response, especially in the frequency range of anomalous propagation. An exact energy balance is formulated which enables the total energy flux at a location either upstream or downstream of the driver to be evaluated. To complement this approach, the ideas of group velocity and wave energy classification are implemented to assess the direction of energy transmission. Thus, for example, a neutrally stable wave is shown to exist downstream of the driver which has positive (downstream-directed) group velocity and yet transmits energy towards the driver. This corresponds to a wave on the lower branch of figure 2*b* in the range $[k_\mathrm{s}, k_\mathrm{p}]$. Crighton & Oswell (1991) explain that because the driver is not the sole source of energy available for transmission to the panel, such counter-intuitive behaviour is acceptable in the system being studied. Furthermore, they calculate the power of the driver and show that in the frequency range $[0, \omega_\mathrm{p}]$ the driver absorbs energy while beyond it the more conventional behaviour of energy input is found. This behaviour is shown to be entirely consistent with their analysis of energy transmission caused by the waves found in each of the upstream and downstream halves of the flexible plate. Their paper is of fundamental importance and concludes with a careful list of the mode types that may be found in each of the upstream and downstream halves of the panel and within each of the frequency ranges demarcated by the values of ω_s, ω_b and ω_p. We will return to these waves later in the present paper.

Further work carried out by Crighton & Oswell has addressed the case of a finite flexible plate. This work is described in Oswell (1992) and summarized by Crighton

(1994). The ends are assumed to be located 'infinitely far' from the driver and the case of free ends is studied. It is shown that the leading and trailing edges of the flexible plate act as wave converters effectively yielding a system with three sources of wave excitation. It will be seen that this multiple-source effect is also found in the present work with fixed panel ends. Crighton (1994) shows that the Crighton & Oswell (1991) analysis can be appropriately applied for the reflected waves either *downstream* of the leading edge or *upstream* of the trailing edge. An additional effect is that the free leading-edge interaction yields reflected waves with greatly increased amplitudes as a result of energy conversion from the mean flow, while the free trailing-edge interaction yields a reduction in reflected-wave amplitudes as energy is propagated downstream of the flexible plate in the wake.

Recent work by Abrahams & Wickham (1994), not yet available in the literature, has contributed to the present problem. In studying the case of continuous oscillatory excitation, Crighton & Oswell (1991) argued that all transients generated in a start-up process would, in the long-time limit, be convected away leaving all parts of the flexible plate responding at the driver frequency. This is true in the absence of absolute instabilities and so Crighton & Oswell focus on a flow speed which is subcritical. Abrahams & Wickham (1994) have included the start-up process wherein all frequencies would be present, and modelled a damped flexible plate. We remark that Brazier-Smith and Scott (1984) did not include flexible-plate damping in their formulation but that a related study by Atkins (1982) found its inclusion to be destabilizing for an 'upstream incoming wave'. Abrahams & Wickham (1994) found that any amount of flexible-plate damping—no matter how small—modifies the morphology of the complex k-plane in their approach and so yields an absolute instability at the point $(k_{\mathrm{p}}, \omega_{\mathrm{p}}^{*})$ in figure 2*b*. This absolute instability would be found at any non-zero flow speed. However, they show that the growth rate of this unstable wave is very small and thus only in the long-time limit would the absolute instability dominate the overall response of the flexible plate. These findings bear a number of similarities with predictions made by Carpenter & Garrad (1986) using the dispersion-relation approach for an infinitely long damped flexible wall. Carpenter & Garrad identify a small positive part to the complex frequency for a wave at k_{p} and recognize that this wave has zero group velocity. This leads them also to speculate that in the long-time limit the flexible-wall response would be dominated by this wave. However, it is only through consideration of both the complex wavenumber and frequency planes that Abrahams & Wickham (1994) have proved that it is an absolute instability. Both Carpenter & Garrad (1986) and Abrahams & Wickham (1994) also suggest that a second wall restorative force, in addition to that provided by bending of the flexible plate, would be required to prevent an infinitely long flexible plate from ultimately succumbing to absolute instability at zero flow speed. However, we note that for times before this absolute instability came to dominate the wave field, the predictions of Crighton & Oswell (1991) would continue to hold.

The present work first attempts to confirm independently the predictions of the theoretical studies discussed above and to visualize the flexible-plate behaviour. However, agreement with the studies of infinitely long flexible plates can only be expected to be limited. Finiteness evidently introduces the possibility of wave reflections at the leading and trailing edges. So too is energy scattering possible. For a flexible panel, even when disturbances are small enough for a linear representation of the wall mechanics to give an accurate approximation, weak nonlinearities due the imposi-

tion of fixed flexible-panel edges have been shown to exist by Garrad & Carpenter (1982*a*) and Lucey & Carpenter (1993*a*). The effects of these nonlinearities are largely confined to regions of the flexible panel close to its leading and trailing edges. As recognized by Crighton (1994), the ability of the two flexible-panel ends to act in a role of wavenumber conversion then yields a system wherein three sources of wave excitation exist in contrast to the single source in the study of an infinitely long panel. The second objective of the present work is to simulate the evolution of disturbances on a flexible panel with fixed ends. In doing so we are able to establish the sequence of events and wave generations that govern the final stages of the hydroelastic instability of small disturbances. A series of numerical experiments is carried out; the results that emerge detail the phenomena that could be anticipated in a physical experiment, albeit an artificial one free of the effects of viscosity. A merit of the numerical simulation is that any linear mechanisms which underly the destabilization process can be identified whereas only the later stages of nonlinear response are most likely to be observed in a physical experiment. Furthermore, the use of a uniform flow in the present paper identifies instability mechanisms that cannot be attributed to viscous effects which would exist in a physical experiment. However, while allowing us to study the practical problem of a flexible panel, the numerical simulation is unable to yield the precise quantitative results which can be achieved in the analyses of an infinitely long flexible plate. Finally, the work of the present paper may also be viewed as a step towards a more complete model of the excited flexible-panel–flow interaction with nonlinear and viscous effects included.

The paper is laid out as follows: in § 2, the governing equations for the wall–flow system are presented and the numerical scheme outlined. The results of numerical experiments are presented in § 3. In the main these pertain to the two-dimensional problem. However, the three-dimensional problem is also addressed and some results are included; the principal purpose of these is to support the validity of the two-dimensional assumption employed herein and in previous work on this problem. Section 4 draws together the overall findings of the present series of numerical experiments and compares these with the relevant aforementioned analytical studies, while § 5 summarizes the most important findings of the present work.

2. Theoretical and numerical model

The governing equation for small displacements, $w(x,t)$, of the flexible plate illustrated in figure 1 can be written as

$$\rho_{\mathrm{m}} h w_{,tt} + d w_{,t} + B w_{,xxxx} = -p(w_{,tt}, w_{,t}, w) + F\cos(\omega_{\mathrm{F}} t)\delta(x - x_{\mathrm{F}})H(t), \qquad (2.1)$$

where ρ_{m}, h, d and B are, respectively, the density, thickness, damping coefficient and flexural rigidity of the panel. An improved, viscoelastic, model of plate damping would employ a complex elastic modulus for the plate material (for example, see Lucey & Carpenter (1995) in the context of flow–structure interaction). However, this approach can only be used when the disturbances are assumed to vary harmonically with time. An important feature of the present approach is that, as in a physical experiment, the disturbances should be permitted to develop with no prescribed restrictions in their form. Accordingly, the simple form of damping shown in equation (2.1) is retained for the present work. On the right-hand side, the action of the fluid flow is represented by the perturbation pressure (per unit width), p,

generated by the dynamic deformation of the flexible panel. This term comprises contributions which may be identified as hydrodynamic inertia ($w_{,tt}$ dependence), damping ($w_{,t}$ dependence) and stiffness (w dependence). This terminology is discussed by Kornecki *et al*. (1976). The second forcing term represents oscillatory line excitation located at x_{F} with frequency and amplitude denoted by ω_{F} and F. The presence of the step-function, H, identifies the starting time of the point driver. In the results that follow, hinged leading and trailing edges are assumed; these require the imposition of $w = w_{,xx} = 0$ at the join to the rigid surface. Alternatively, 'built-in' leading and trailing edges could be modelled readily—and their effects have also been studied—by modifying this condition to $w = w_{,x} = 0$ at the panel ends.

To obtain the fluid pressure, we assume unsteady potential flow governed by the Laplace equation:

$$\nabla^2 \Phi = 0, \tag{2.2}$$

where Φ is the perturbation potential with the total flow field given by $\boldsymbol{U} + \boldsymbol{\nabla}\Phi$. The kinematic boundary condition at the wall–flow interface, moving with velocity $\boldsymbol{u}_{\mathrm{s}}$, is

$$\boldsymbol{U} \cdot \boldsymbol{n} + \boldsymbol{\nabla}\Phi \cdot \boldsymbol{n} = \boldsymbol{u}_{\mathrm{s}} \cdot \boldsymbol{n}, \tag{2.3}$$

where $\boldsymbol{n}$ is the unit vector normal to the wall. Upon solution for Φ, the perturbation pressure can be found through the unsteady Bernoulli equation:

$$-p = \rho \left\{ \frac{\partial \Phi}{\partial t} + \tfrac{1}{2}(\boldsymbol{U} + \boldsymbol{\nabla}\Phi) \cdot (\boldsymbol{U} + \boldsymbol{\nabla}\Phi) - \tfrac{1}{2}\boldsymbol{U} \cdot \boldsymbol{U} \right\}. \tag{2.4}$$

Solution of the Laplace equation is achieved by a distribution of source-sink singularities of strength $\sigma(s)$ (here s is a wall-fitted tangential coordinate) over the interface. The perturbation potential is then given by

$$\Phi(\boldsymbol{x}) = \frac{1}{2\pi} \int_{\ell} \sigma(s) \ln |\boldsymbol{x} - \boldsymbol{x}_{\mathrm{s}}| \, \mathrm{d}s, \tag{2.5}$$

where $\boldsymbol{x} = (x, y)$ is a general vector location in the fluid and $\boldsymbol{x}_{\mathrm{s}}$ lies on the fluid boundary, ℓ. Imposition of the kinematic boundary condition (equation (2.3)) and proper treatment of the singularity at $\boldsymbol{x} = \boldsymbol{x}_{\mathrm{s}}$ leads to the following integral equation which determines the singularity strength distribution, $\sigma(s)$:

$$\tfrac{1}{2}\sigma(\boldsymbol{x}_{\mathrm{s}}) + \frac{1}{2\pi} \int_{\ell : \boldsymbol{x} \neq \boldsymbol{x}_{\mathrm{s}}} \sigma(s) \frac{\partial}{\partial n} (\ln |\boldsymbol{x} - \boldsymbol{x}_{\mathrm{s}}|) \, \mathrm{d}s = (-\boldsymbol{U} \cdot \boldsymbol{n} - \boldsymbol{u}_{\mathrm{s}} \cdot \boldsymbol{n}), \tag{2.6}$$

the differentiation being in the direction normal to the wall. Equation (2.6) is solved by discretizing the fluid boundary into a collection of surface panels and then satisfying the no-flux condition only at the panel control points, here assumed to lie at the panel centres. This method was first presented by Hess & Smith (1967). Thereafter, Φ can be assembled from the discretized form of equation (2.5) and the perturbation pressures at the panel control points obtained from equation (2.4).

The solution method for the fluid, outlined above, is equally applicable to linear and nonlinear deformations of the interfacial boundary. However, for nonlinear waves, the structural side of the wall equation (2.1) would require modification to include the effects of induced tension and curvature in the bending–stiffness term. The present paper is confined to an investigation of small disturbances of the wall. To reduce the computational effort, a linear boundary-element (or 'panel') method has been

used. Thus, the integrals need only be carried out over the flexible part of the wall–flow interface. To increase the accuracy of the solution without recourse to very fine discretizations, a higher-order boundary-element method has been implemented. Details of the method may be found in Lucey & Carpenter (1992*a*) and Lucey (1989).

The numerical method used to solve the present flexible-wall–flow system employs a finite-difference representation of equation (2.1). The flexible surface is discretized into a set of mass points which coincide with the panel ends used for the boundary-element method. Linear interpolation is used to find the hydrodynamic pressure at the mass points and the driver force added in at the appropriate mass point. A semi-implicit time-stepping method, described in Lucey & Carpenter (1992*a*), is then used to determine the evolution of disturbances on the flexible panel.

Finally, the non-dimensionalization scheme follows that introduced by Crighton & Oswell (1991). The non-dimensional flow speed, excitation force and damping coefficient are defined by

$$U' = \left\{\frac{(\rho_{\mathrm{m}}h)^{3/2}}{\rho B^{1/2}}\right\}U, \tag{2.7\,a}$$

$$F' = \left\{\frac{(\rho_{\mathrm{m}}h)^{2}}{\rho^2 B}\right\}F, \tag{2.7\,b}$$

$$d' = \left\{\frac{(\rho_{\mathrm{m}}h)^{3/2}}{\rho^2 B^{1/2}}\right\}d, \tag{2.7\,c}$$

while non-dimensional frequencies and wavenumbers are given by

$$\omega' = \left\{\frac{(\rho_{\mathrm{m}}h)^{5/2}}{\rho^2 B^{1/2}}\right\}\omega, \tag{2.8\,a}$$

$$k' = \left\{\frac{\rho}{\rho_{\mathrm{m}}h}\right\}k. \tag{2.8\,b}$$

In the results that follow, we will continue to use $\rho_{\mathrm{m}}h/\rho$ as the length-scale and $(\rho_{\mathrm{m}}h)^{5/2}/\rho^2 B^{1/2}$ as the time-scale.

3. Results of numerical experiments

Crighton & Oswell (1991) noted that non-dimensionalization reduces the system of equations governing the behaviour of the infinite flexible-plate–flow system to one with a single parameter, namely the dimensionless flow speed, when the fluid is incompressible. We follow Crighton & Oswell and focus on the system response at the flow speed $U' = 0.05$ which is below the critical velocity, $U'_{\mathrm{c}} = 0.074$, for absolute instability in their, and Brazier-Smith & Scott's (1984), analysis. To facilitate a suitable comparison, the flexible plate is undamped over most of its extent for the results presented below. However, heavy damping is included near the leading and trailing edges. This is done in conjunction with the choice of a long panel†. Thus, for early times after start-up, the present numerical experiments should yield results which can be compared with the theoretical predictions for an infinitely long flexible plate. Thereafter, departures from the behaviour of an infinitely long system may be expected. In the later phase of the finite-system response, where wave reflections

† Hereafter we will refer to the present finite-length flexible plate as a 'panel'.

and wavenumber conversions may be occurring at the panel ends, it may be thought that the inclusion of this heavy damping exercises a significant effect. Accordingly, numerical experiments have also been carried out with uniformly distributed plate damping and for a wholly undamped panel. The results of these numerical experiments, although not formally presented, will be discussed as departures from the basic configuration. We wish to emphasize that the features found in the results presented here, for an essentially undamped panel, are also typical of the responses of damped panels thereby eliminating the effect of damping as a key ingredient in the structural modelling. Most of the results presented here pertain to a single panel length. However, all of the following simulations have been repeated using a longer panel so that any features of the response dependent upon panel length may be identified.

As stated above, the key variable in the wall–flow system is the flow speed. Throughout the following results, a non-dimensional flow speed of $U' = 0.05$ is used. In order to give an engineering 'feel' for dimensional system parameters, this can be equated to a water (density $\rho = 1000\,\mathrm{kg\,m^{-3}}$) flow of $U = 0.908\,\mathrm{m\,s^{-1}}$ over an aluminium (elastic modulus, $E = 70\,\mathrm{MPa}$; Poisson ratio, $\nu_\mathrm{p} = 0.3333$; density, $\rho_\mathrm{m} = 2710\,\mathrm{kg\,m^{-3}}$) panel of thickness $h = 5\,\mathrm{mm}$. When using these wall and fluid properties, the frequency bounds, ω_s and ω_p, of Crighton & Oswell's (1991) region of anomalous propagation, respectively, take the dimensional values 3.027 and $3.169\,\mathrm{rad\,s^{-1}}$. The non-dimensional time period, ΔT, used throughout this paper, represents 1340 of the natural non-dimensional time units discussed in § 2. The size of ΔT is better appreciated as closely approximating a half wave period at ω_p. Alternatively, for the physical data suggested above, the dimensional value of ΔT is exactly 1 s.

The heavy damping adjacent to the leading and trailing edges which is present in the basic configuration of an otherwise undamped plate, covers 5% of the panel length, L. In the basic configuration, the panel has dimensional length $L = 10\,\mathrm{m}$, which gives $L' = 738$. For the aluminium panel suggested above, this is equivalent to about eight wavelengths with wavenumber k_p. In simulations for which distributed damping has been included, a range of values has been tested. This range covers values from zero up to a maximum non-dimensional coefficient, $d' = 5.5 \times 10^{-4}$. The upper limit represents an attenuation of approximately a half wave amplitude per cycle at the frequency ω_p. This maximum value is far in excess of that which could be associated with the sample physical data given in the preceding paragraph. The purpose of exploring such artificially high values is to identify any dependence of response on flexible-plate damping.

Analysis of the data provided by each numerical experiment is carried out in a number of ways. The displacement of a single panel point can be monitored during the passage of time. This has been recorded for two points which are $\pm 0.2L$ from the driver. Power spectra of the time-series that are captured then yield the frequency components of the disturbances at these points. Instantaneous wall profiles (or 'snapshots') at different times in the simulation provide a visual impression of the wave response. Power spectra of these—carried out separately for the upstream and downstream halves—yield the wavenumber components of the response at the particular time. Together with frequency components prevalent at the specified time and location, (k, ω) data can be collected to be compared with those predicted by the dispersion diagram. In addition to the visual data provided by the snapshots

of the panel deflection, further elucidation of the character of the dominant waves in the upstream and downstream of the driver is provided by flexible-plate energy measurements. For each half of the panel, the strain, E_{S}, kinetic, E_{K}, and total, E_{T} $(= E_{\mathrm{S}} + E_{\mathrm{T}})$ energies are calculated at each time step of the simulation. A further energy quantity described as the 'virtual work done by the hydrodynamic stiffness', E_{VW}, is also evaluated. The dimensional energy terms are calculated through the following expressions:

$$E_{\mathrm{S}} = \frac{1}{2} B \int w_{,xx}^2 \, \mathrm{d}x, \tag{3.1 a}$$

$$E_{\mathrm{K}} = \frac{1}{2} \rho_{\mathrm{m}} h \int w_{,t}^2 \, \mathrm{d}x, \tag{3.1 b}$$

$$E_{\mathrm{VW}} = -\frac{1}{2} \int w p(0, 0, w) \, \mathrm{d}x. \tag{3.1 c}$$

The quantity E_{VW} was introduced by Lucey & Carpenter (1992*a*); it can be interpreted as an averaged measure of the hydroelastically destabilizing forces applied to the flexible wall by the pressure. When this term exceeds the strain energy, the flexible-wall deformation is such that self-sustaining hydroelastic instability of a panel can exist. We remark that, in common with aero/hydroelastic studies of panels, such criteria only provide an overall indication of whether the panel is unstable. In an engineering context, a sustained growth of panel energy is the principal concern. Further to the identification of such instabilities, the energy records are able to give a comparative measure of the severity of the instability.

The above energy considerations provide a means of recognizing overall instability of a panel. Of scientific interest is the identification of the detailed wave behaviour that constitutes the overall instability mechanism. The methods described above are insufficient to provide details of energy flux, group velocity or wave energy classification in the formal manner presented by Crighton & Oswell (1991) for an infinitely long flexible plate. Moreover, the present numerical approach does not permit evaluations of fluid-energy terms and so we cannot ascertain, for example, the total energy flux associated with the simultaneous propagation of waves in both media of the coupled system. Instead, the present work necessarily focuses on the panel alone (with the fluid-flow effects included) and adopts methods closer to those found in physical experiments. Our restricted goal, then, is to expose sequences of panel deformations and energy fluxes within the panel that would characterize its behaviour and which might be observed in a physical experiment. Thus, we also generate data for the evolution of the spatial distribution of wall energy along the panel. This can be done for the driver running continuously or with the driver switched off at some time during the simulation. The switch-off experiment is then able to determine the propagation direction of a disturbance and approximate its propagation speed. Thus, the propagation of unstable waves found in the present work can be classified as convective or absolute using the criteria presented in the ray diagrams of Huerre & Monkewitz (1990).

Other data collected include a record of the power input by the driver against time along with the rate of energy dissipation by the heavy damping adjacent to the panel's leading and trailing edges. Finally, to assist in the understanding of all of the numerical experiments, computer-generated moving images have been made

which, at least approximately, simulate a physical experiment; these are useful in qualitatively identifying wave phase velocities.

Before moving to the results, it is noted that the numerical simulation has been thoroughly tested to verify the integrity of the method and determine the required mesh resolution; this task is documented in Lucey (1989). For the present use of the method, simulations have been carried for a driven panel *in vacuo* and in the presence of a fluid with $U' = 0$. For the range of frequencies and wavelengths typical of the following investigation, excellent agreement is found with the appropriate dispersion diagrams wherein there is reflectional symmetry in the wavenumber axis. The continuous power input by the driver is transmitted out to the leading and trailing edge damping zones by the flexural waves. The rate of dissipation in these zones exactly balances the driver input and a steady state is established. Thus, for conventional flexural waves, the present panel behaves in a manner identical to that of an infinitely long flexible plate.

(*a*) *Two-dimensional simulations*

Results of two numerical experiments are presented here. These are described below under the subheadings 'low-frequency excitation' and 'high-frequency excitation'. The results typify, respectively, the panel behaviour in each of the ranges of excitation frequency, ω_F, given by $0 < \omega_F < \omega_p$ and $\omega_p < \omega_F$. The non-dimensional value of ω_p is 0.002365 and, as can be seen in figure 2*b*, it is the frequency associated with the maximum on the lower branch of the dispersion curve.

(i) *Low-frequency excitation:* $\omega_F = 0.001492$

Presented in figure 3*a–e* are snapshots of the wall deflection at times $4\Delta T$, $8\Delta T$, $10\Delta T$, $14\Delta T$ and $16\Delta T$ after start-up of the driver which is located at the panel midchord. Energy records for each of the upstream and downstream halves are given in figure 4*a, b*. In figure 5 we record the principal waves found, as approximate $(k, \mathrm{Re}(\omega))$-data, at different times of the numerical simulation on the background of a dispersion curve. Each wave has an alphabetic label which is assigned in the description that follows below.

For early times of the numerical simulation, the wall behaviour is typified by the plot at $t' = 4\Delta T$. Downstream of the driver, a spatially growing unstable wave is found (wave A). This ties in with the prediction of convective instability by Crighton & Oswell (1991) except that the frequency of the response is different from that of the driver; it is, in fact, substantially higher. This difference in frequency owes its existence to the start-up process and persists indefinitely. In contrast, the analysis by Crighton & Oswell is based upon the assumption that the response and drive frequencies are identical. Other simulations at lower driver frequencies than the present one also show the same feature and very similar response frequency. Presumably, the most amplified wave is selected from the wave packet generated in the start-up process. In the upstream half two waves can be discerned. One (wave B) is the anticipated upstream-travelling modified flexural wave associated with $-\omega_F$ of the dispersion curve included in figure 5. (Throughout this paper we will continue to use the description 'modified flexural waves' as shorthand for 'fully coupled fluid loaded structural waves with mean flow'.) The second (wave C), is a downstream-travelling wave which has a lower wavenumber than the first and can be associated

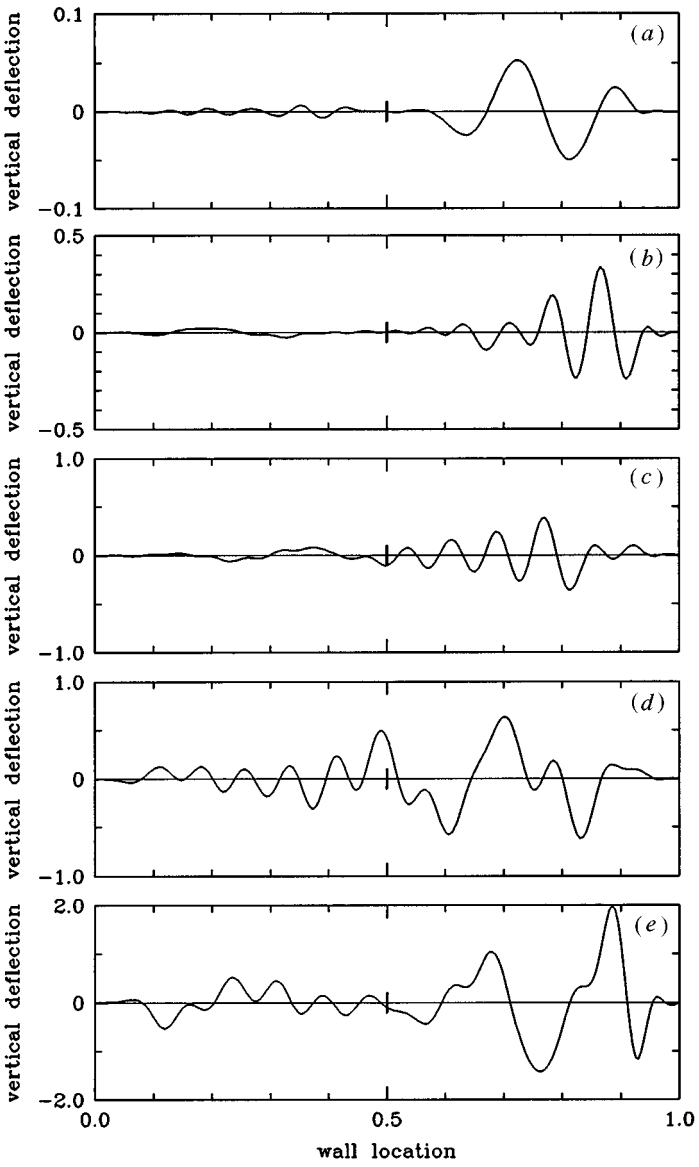

Figure 3. Low-frequency excitation ($\omega_F = 0.001492$). Instantaneous wall profiles for $U' = 0.05$ at different times: (*a*) $t' = 4\Delta T$; (*b*) $t' = 8\Delta T$; (*c*) $t' = 10\Delta T$; (*d*) $t' = 14\Delta T$; (*e*) $t' = 16\Delta T$.

with $\mathrm{Re}(\omega) > 0$ on the lower branch of the dispersion relation. The upstream energy record at early times indicates that wave C is hydroelastically unstable although there is not firm evidence of exponential growth. We can show that wave C propagates wall energy density in the upstream direction and has the same identity as the wave illustrated and discussed in figure 7. In contrast, the downstream energy record evinces definite growth of wall energy associated with the spatially growing instability, wave A.

In order to elucidate the character of the spatially growing wave (A) in the down-

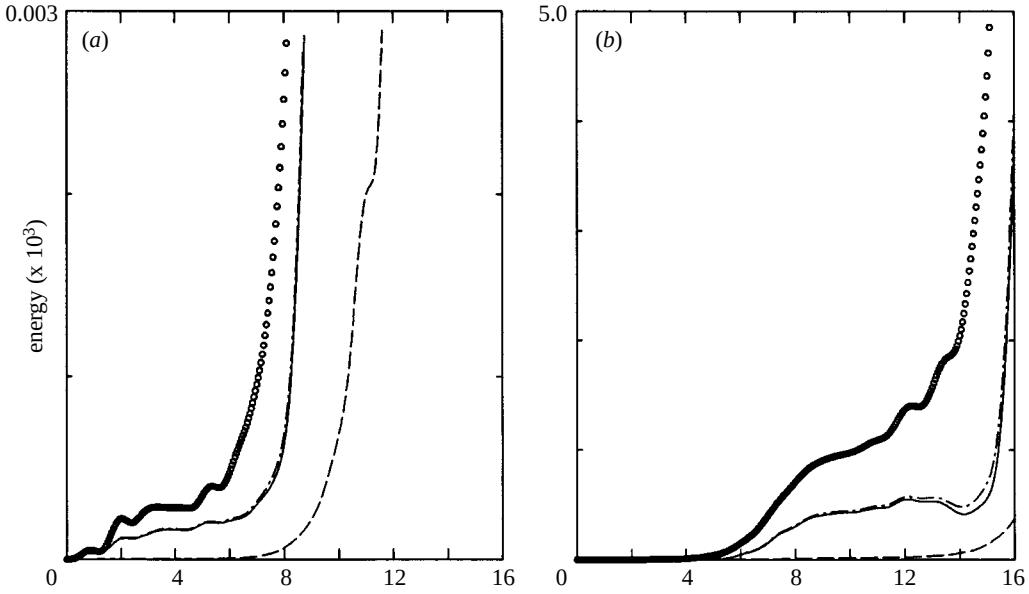

Figure 4. Energy records for low-frequency excitation for (a) upstream of driver and (b) downstream of driver: ——, strain energy, E_{S}; – – –, kinetic energy, E_{K}; – · – · –, total energy, E_{T}; ○, virtual work done by the hydrodynamic stiffness, E_{VW}.

stream half of the panel, a further numerical experiment was undertaken. The same parameters were used as for figure 3 except that for this simulation the driver was switched off at $2\Delta T$. The choice of $2\Delta T$ ensured that the wavefront had not yet reached the trailing edge of the panel. The purpose of this experiment was to remove the source of the wave and monitor its ensuing development. However, in this experiment, it emerged that disturbances already excited in the upstream half of the panel were able to act as a disturbance source for wave A. The effective origin of this wave then quickly moved upstream until a steady state was established whereby the leading edge became the source of the wave. To prevent this happening, we artificially introduced heavy damping in the upstream half of the panel at the same time as switching off the driver. The results of this modified experiment are presented in the waterfall diagram of figure 6. Plotted there is the wall strain-energy density in the downstream half of the flexible panel. Plots of total wall energy density showed similar features but were marred by high-frequency transients generated by the sudden artificial imposition of the high plate damping in the upstream half at $2\Delta T$. Note that at the later times shown in figure 6, a high value of wall energy density is accumulating at the trailing edge of the panel and that this is associated with a wave of different periodicity. It is evident from figure 6 that the wave behaves like a convective instability. Sketched in figure 6 are suggested rays of propagation for the wave packet. From these rays an estimation of the non-dimensional mean propagation speed of the wall energy density is found to be 0.043. This value shows agreement with the group velocity of 0.045 prevailing in the modal-coalescence region of the dispersion diagram of figure 2*b*. For the panel length chosen for this simulation we also note that, at the experimentally determined propagation velocity of 0.043,

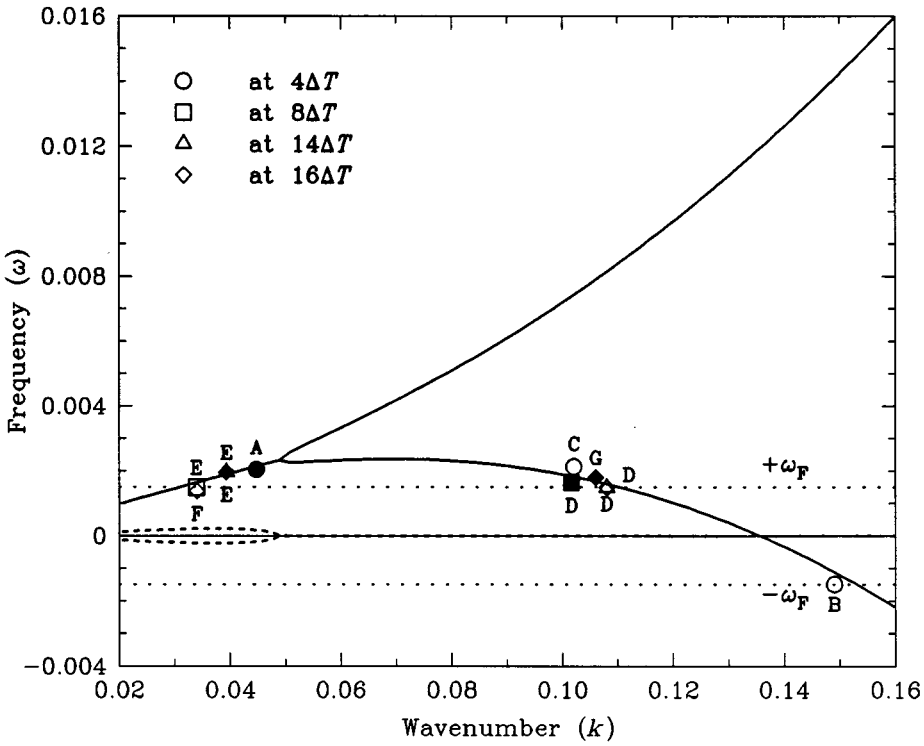

Figure 5. Locations of waves seen in figure 3 plotted in the k–ω plane together with the dispersion curve and value of excitation frequency, ω_{F}: open symbols, upstream response; filled symbols, downstream response. Alphabetic labels of data points are referenced in the text.

the wall energy carried by wave A would reach the trailing edge at approximately $t' = 6\Delta T$.

Figure 3*b*, at $t' = 8\Delta T$, illustrates the next stage of the panel response. In the downstream half, a new unstable wave (wave D) of shorter wavelength has developed from the trailing edge. This wave can be identified with the branch $[k_{\mathrm{p}}, k_{\mathrm{c}}]$ of the lower branch of the dispersion curve plotted in figure 2*b*. Moving images confirm that it is a downstream travelling wave. However, the wall energy density propagation of this disturbance is in the upstream direction, as can be seen in the waterfall diagram of figure 7 which covers its development for times t':$8\Delta T \rightarrow 10\Delta T$. In this diagram the sums of wall strain- and kinetic-energy densities are plotted for the downstream half of the panel. Suggested rays for the wave packet have been sketched in. Two features are apparent in this diagram. First, the growth rate of the dominant wave component is small and secondly, the instability is convective in that it propagates upstream. The non-dimensional mean propagation speed has been estimated as 0.043. We note that this value and the direction of propagation corresponds with a group velocity of -0.040 found on the dispersion diagram of figure 2*b* at the k-value of wave D. Although the growth rate of wave D is lower than that of wave A found in the initial stages—a feature observable in the time range t':$8\Delta T \rightarrow 12\Delta T$ of the energy record—it becomes the dominant wave in the downstream half. This phenomenon ties in with the convective nature of wave A which is limited by the panel length in its ability to convert fluid energy to wall energy. In the upstream half, a new wave (wave E)

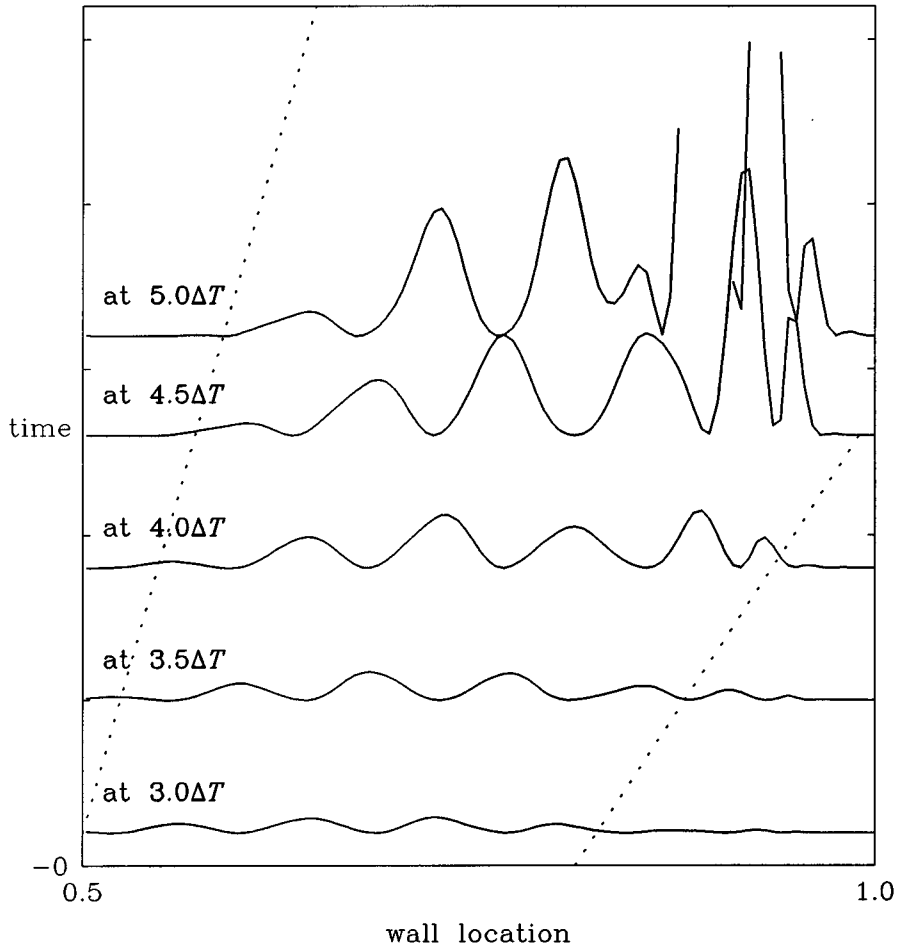

Figure 6. Evolution of wall strain-energy density for the wave type found downstream of the driver in figure 3*a*. In this simulation the driver has been switched off at $t' = 2\Delta T$ otherwise the parameters are identical to those of figure 3.

has also developed. This appears to originate at the leading edge and represents a spatially growing instability of the same type as wave A found at early times in the downstream half. That it is an unstable wave is confirmed by the upstream energy record. In addition to the above waves, power spectra—not presented here—identify a response component at ω_{p}^*, and the associated wavenumber, located in the central part of the panel. As recognized by Abrahams & Wickham (1994), this corresponds to an absolute instability. It originates in the start-up process and shows little spread away from its point of initiation. Low-intensity traces of this wave continue to appear in the power spectra through all stages of the panel's response. In this low-driver-frequency experiment the growth rate of this ω_{p}^* wave is so small as to render it insignificant alongside the dominant effects of the spatially growing instabilities which are concurrently present. However, it will be seen that it plays an important role in the destabilization process of the panel when a high-frequency excitation is used.

At $t' = 10\Delta T$ (figure 3*c*) the upstream-propagating wave D, discussed above, has

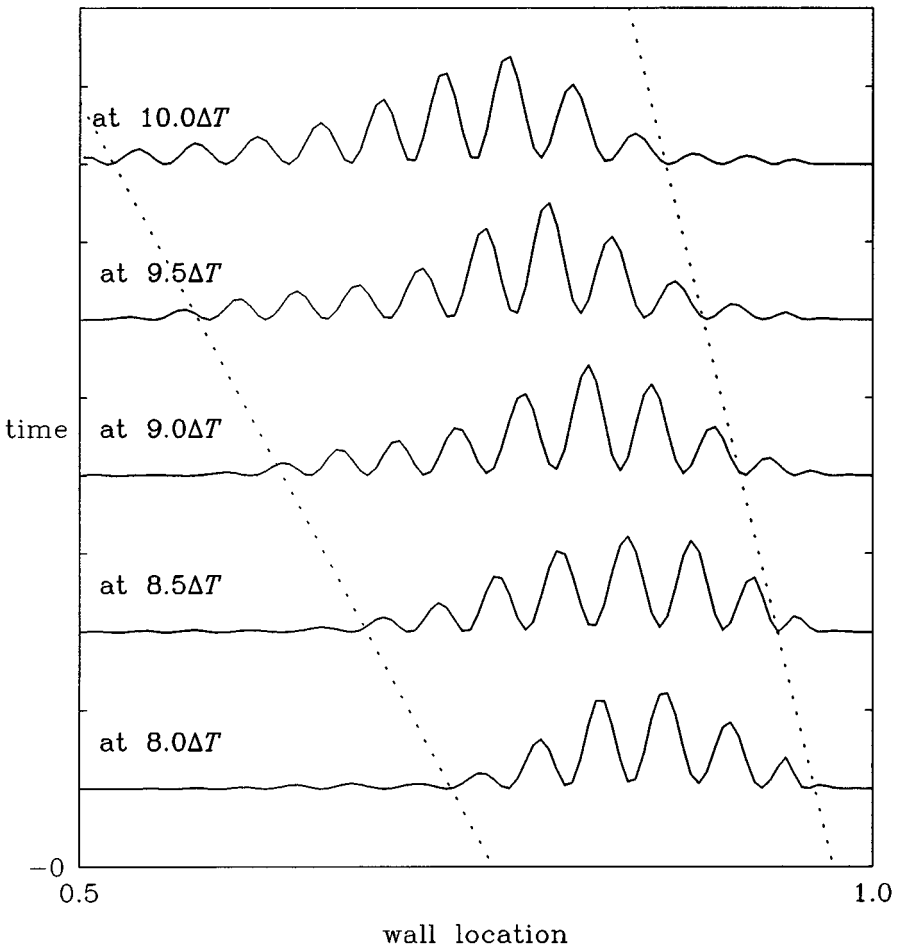

Figure 7. Evolution of the total wall energy density for the wave type found downstream of the driver in figure 3*b*, *c*.

come to occupy most of the downstream half of the panel. Following this stage, figure 3*d*, plotted at $t' = 14\Delta T$, indicates a dramatic change in the instability mechanism. The upstream-propagating wave D has migrated through to the upstream half of the panel and has effectively supplanted the long-wavelength disturbance (wave E) which appeared at earlier times. This behaviour is consistent with the estimated mean propagation speed of the disturbance; at a speed of 0.043, the time difference between figure 3*c* and 3*d* translates into a propagation distance of about one-third of the panel length, L. The spatially growing wave E, triggered by the leading edge, has now penetrated the downstream half where it becomes the dominant wave. This is a far more unstable wave, as is evidenced by the downstream energy record for times after its establishment at $t' = 14\Delta T$. For the plot at $t' = 16\Delta T$ (see figure 3*e*) continuous growth of this wave is occurring in the downstream half. Upstream of the driver another wavenumber conversion has taken place. The upstream-propagating wave D interacts with the leading edge and launches another downstream-propagating instability, denoted wave F. We note that the timing of this interaction is again consistent

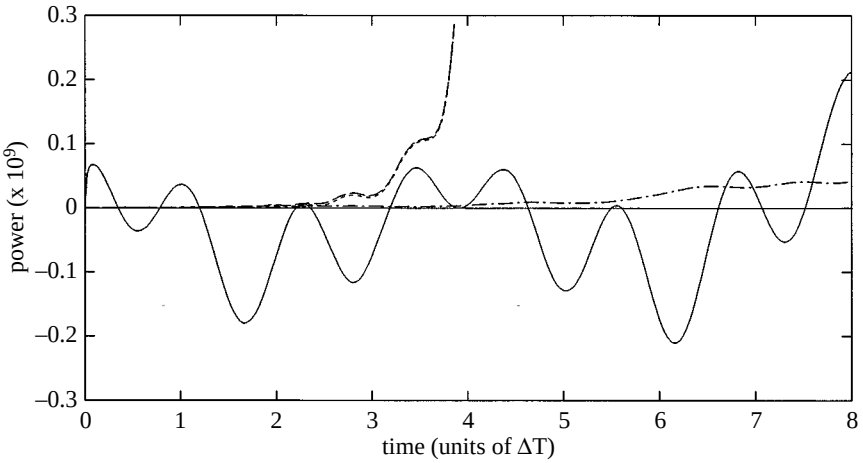

Figure 8. Records of driver power and energy-dissipation rate at the panel ends for low-frequency excitation: ——, driver power; – – –, total dissipation rate at panel ends; – · – · –, dissipation rate at upstream end; - - - -, dissipation rate at downstream end.

with the progress of the upstream-propagating wave D; the measured mean propagation speed suggests a convection distance of $0.7L$ between the disturbance location seen at $t' = 8\Delta T$ (figure 3*b*) and $16\Delta T$ (figure 3*e*). Similarly, the spatially growing wave E that appeared at $t' = 8\Delta T$ has reached the trailing edge at $t' = 16\Delta T$ and can be seen in figure 3*e* to be exciting a new wave (wave G) of shorter wavelength which has the same properties as the upstream-propagating wave D featured in the waterfall diagram of figure 7.

Thus a pattern of behaviour is set up. Two broad types of wave dominate the panel response. These we will term type I and type II. Both type I and type II are downstream-travelling waves and the disturbances are convectively unstable. Contrasting the two, type I has a long wavelength, high growth rate and propagates wall energy density in the downstream direction, while type II propagates wall energy density in the upstream direction, has shorter wavelength and a smaller growth rate. Waves A, E and F are type I and waves C, D and G are type II. The repeated exchanges between type I and type II waves ensure disturbance growth at all locations of the panel and yield globally unstable (in the terminology of Akhieser & Polovin (1971)) behaviour of the flexible panel. The importance of the type II wave is not that it significantly contributes to the overall growth of panel energy (its growth rate is very small), but that it transmits wall energy in the upstream direction. Upstream-travelling modified flexural waves, excited by the driver or the trailing edge of the panel, are also capable of transmitting wall energy upstream. However, modified flexural waves would be eliminated by panel damping in a real situation whereas the type II wave is largely unaffected by damping. The driver appears to exercise very little influence once the wave conversions get under way and thus the evolution identified above holds for all excitation frequencies in the range $0 < \omega_{\mathrm{F}} < \omega_P$. Moreover, once the effects of panel finiteness have taken effect, the driver can be switched off with little modification to the ensuing sequence of events. For the present numerical experiment the presence of the driver is insignificant after approximately $8\Delta T$.

In figure 8, a record of the driver power and rate of dissipation at the panel ends

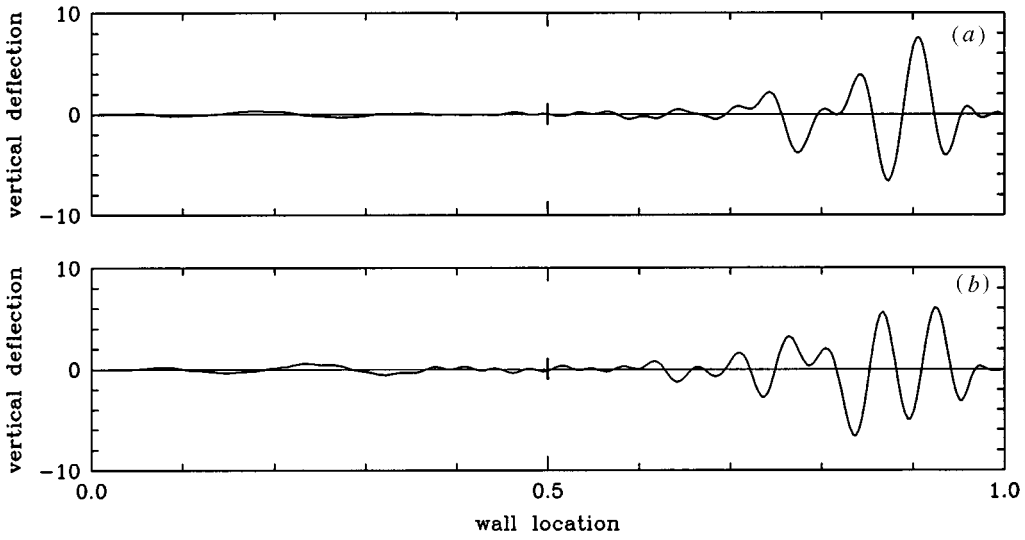

Figure 9. Instantaneous wall profiles at different times for low-frequency excitation. The panel length is $1.5L$; otherwise the parameters are identical to those of figure 3: (*a*) $t' = 11\Delta T$; (*b*) $t' = 12\Delta T$.

is presented for the time range t':$0 \rightarrow 8\Delta T$. It is immediately evident that, after start-up, the driver absorbs energy as predicted by Crighton & Oswell (1991).

An equivalent numerical expriment has been carried using a panel of length $1.5L$ instead of L. In figure 9*a*, *b*, we present two snapshots which are obtained at times $t' = 11\Delta T$ and $t' = 12\Delta T$. At early times, the longer panel behaves in a manner identical to that of the shorter panel which was described at length above. However, the stage characterized by the spatially growing wave (type I), clearly evident in figure 3*a*, has a greater timespan in the case of the longer panel. On this longer panel, it also gives way to the type II shorter-wavelength disturbance capable of propagating wall energy density in the upstream direction. Its appearance is evident in figure 9*a* which is very similar to the shorter panel's development between $t' = 7\Delta T$ and $8\Delta T$ (the latter is plotted in figure 3*b*). This time difference agrees with approximate predictions obtained by considering the mean wall energy density propagation speed estimated for the type I wave of figures 3*a* and 6. The non-dimensional value of 0.043 would imply a time delay of about $3\Delta T$ in the launch time of the type II wave on this longer panel. This verifies the assertion that the type II wave is generated at the trailing edge by the arrival of the type I wave. A similar effect is found in the upstream half of the panel; the emergence of the wave seen in figure 9*b* can be compared with that of figure 3*b*. The time delay in its appearance—when contrasting numerical experiments for the two panel lengths—can be closely predicted using a mean wall energy density propagation speed for the type II wave which, at the start of the simulation, emanates from the driver. Thus, for the response evolution, the only difference engendered by increasing the panel length is that longer times occur between the wave conversions, owing to panel edges, that were discussed in detail for the standard length.

The complete exclusion of damping throughout the panel makes little difference to the pattern of wave generation and growth of wall disturbances identified for

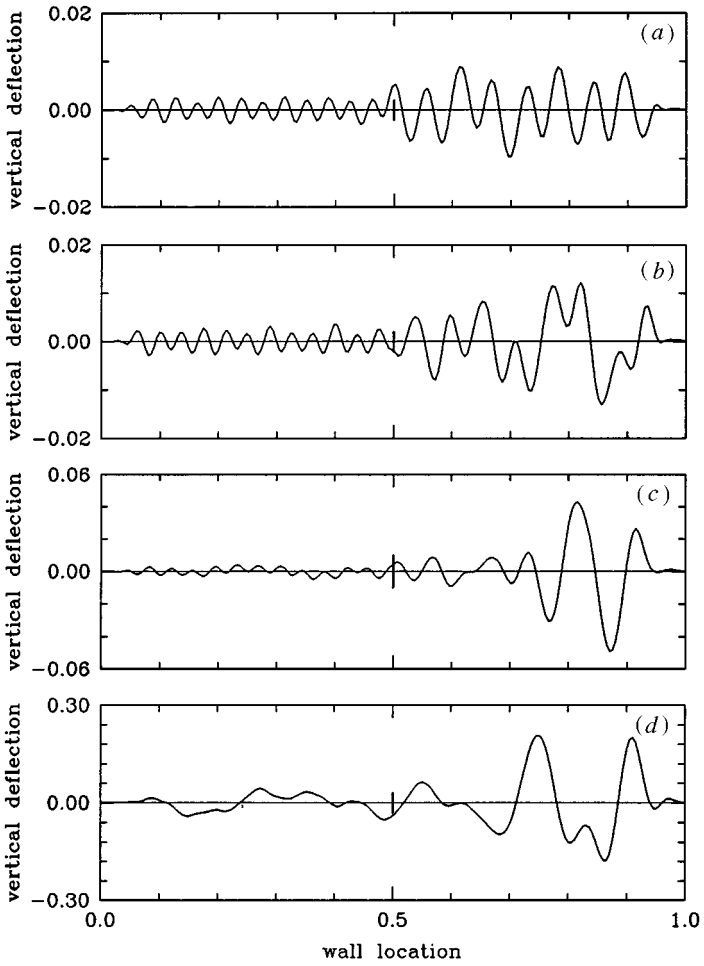

Figure 10. High-frequency excitation ($\omega_F = 0.01343$). Instantaneous wall profiles for $U' = 0.05$ at different times: (*a*) $t' = 2\Delta T$; (*b*) $t' = 4\Delta T$; (*c*) $t' = 8\Delta T$; (*d*) $t' = 16\Delta T$.

the basic configuration. However, a high-frequency response is superimposed upon the panel deformations seen in figure 3*a–e*. For example it is noted that upstream-travelling modified flexural waves, consistent with the dispersion diagram, may be initiated by the trailing edge. Furthermore, the absence of plate damping appears to facilitate the establishment of the longer-wavelength type I instability manifest upstream of the driver in figure 3*e*. As a consequence, disturbance amplitudes at $t' = 16\Delta T$ are greater upstream of the driver when compared with those downstream of the driver†. In a similar numerical experiment in which distributed panel damping is used, again there is little departure from the wave evolution found for the basic configuration. However, like the zero-damping case, it is found that in the late stages, wave amplitudes upstream exceed those found downstream of the driver. In the basic configuration, with heavy damping adjacent to the leading edge, we may then

† It is, of course, recognized that the entire absence of damping means that energy input by the driver may be trapped in a finite panel and lead to amplitude growth of neutrally stable waves.

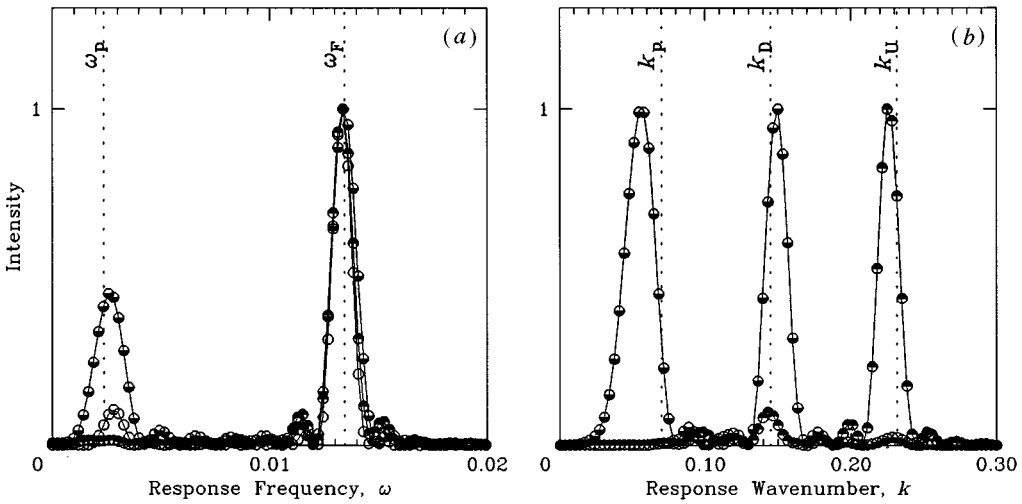

Figure 11. Power spectra associated with the response to high-frequency excitation: (*a*) ω-spectrum for t':0 $\rightarrow 4\Delta T$; (*b*) k-spectrum at $t' = 4\Delta T$. Legend: panel response at: ○, mid-point; ◓, upstream of driver; ◒, downstream of driver. ω_F is the driver frequency, (k_p, ω_p) is the maximum on the lower branch and k_U and k_D are, respectively, the wavenumbers of the modified flexural waves, upstream and downstream of the driver, predicted by the dispersion-relation approach.

question its apparent role in partially inhibiting or delaying the formation of the type I instability that is launched by the arrival of wall energy propagated in the upstream direction by the type II wave. In fact, it suggests that the type II wave is attenuated by the heavy damping so reducing its effectiveness in providing energy for the wave conversions. Furthermore, these further numerical experiments have shown that the growth of the type II wave is not a result of wall damping. On the contrary, wall damping acts in its conventional role of reducing the growth rates of both the type I and type II unstable wall waves. We may therefore conclude that panel damping does not play any significant part in the destabilization mechanisms of a panel with fixed leading and trailing edges.

(ii) *High-frequency excitation:* $\omega_F = 0.01343$

Figure 10*a–d* shows snapshots of the wall deflection at times $2\Delta T$, $4\Delta T$, $8\Delta T$ and $16\Delta T$. Again, these times have been selected because each represents a distinct step in the overall evolution of the panel's response. In figure 10*a*, the panel response is seen to be one of modified flexural response. Neutrally stable waves (waves J and K) travel out from the driver and are attenuated in the regions of heavy damping adjacent to the panel ends; thus, after start-up a steady state has been established which is entirely in agreement with the waves at this frequency predicted by the dispersion diagram. However, there is some evidence of wave modulation in both halves of the panel. This is particularly pronounced in deflection time-histories of single points on the panel (not presented here). The wave amplitude is smaller upstream of the driver because the upstream travelling wave has a larger absolute value of group velocity, so activating the leading-edge damping sooner.

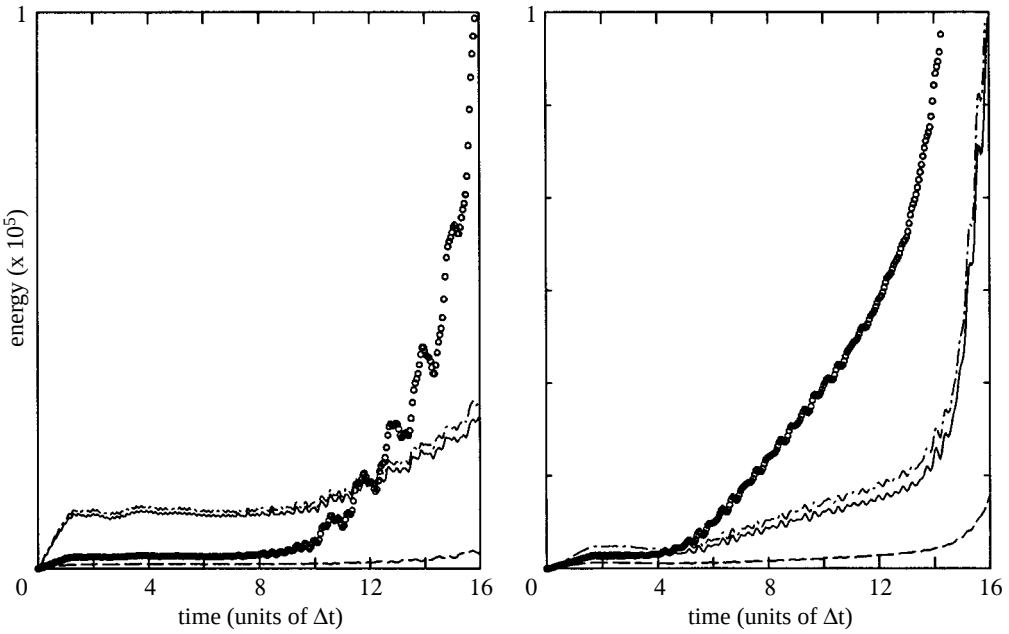

Figure 12. Energy records for high-frequency excitation (a) upstream of driver and (b) downstream of driver: ——, strain energy, E_{S}; – – –, kinetic energy, E_{K}; – · – · –, total energy, E_{T}; ∘, virtual work done by the hydrodynamic stiffness, E_{VW}.

Following from the above, figure 10b at $t' = 4\Delta T$, shows that the growth of the modulation is such that downstream of the driver a new wave (wave M) has developed. Upstream of the driver, the modulation noted at $t' = 2\Delta T$ is more prominent. Figure 11a, b shows power spectra for the frequency and wavenumber associated with times t':$0 \rightarrow 4\Delta T$ and the wall profile seen in figure 10b. In addition to the signal at ω_{F}, a further low-frequency wave has been excited in the start-up process. At these early times, wave M appears in the downstream half of the panel although at later times it can also be identified upstream of the driver. Associated with this new frequency is the lower wavenumber, k_{p}, which appears in figure 11b along with the wavenumbers, k_{d} and k_{u}, of the expected modified flexural response (waves J and K). The energy records for this numerical experiment are shown in figure 12a, b; the downstream half of the panel shows an increase setting in at about $t' = 4\Delta T$ after a period of steady-state behaviour. Thus the new low-frequency wave M that has appeared represents a hydroelastic instability. The location of wave M in the (k, ω)-plane can be seen in figure 13. It is significant that it lies very close to the point $(k_{\mathrm{p}}, \omega_{\mathrm{p}}^*)$ where the group velocity is zero. That it owes its origin entirely to preferential amplification in the start-up process has been verified by repeating the numerical experiment with a panel of length $1.5L$. The corresponding power spectra are identical to those discussed above, as are the deflection profiles at these early times. Thus, the selection of this frequency very close to ω_{p}^* is neither an overall resonance of the system nor an effect generated at the leading and trailing edges. It is also recorded that similar numerical experiments using a panel comprising a flexible plate which is either wholly undamped or has uniformly distributed damping, yield almost identical results to those presented here.

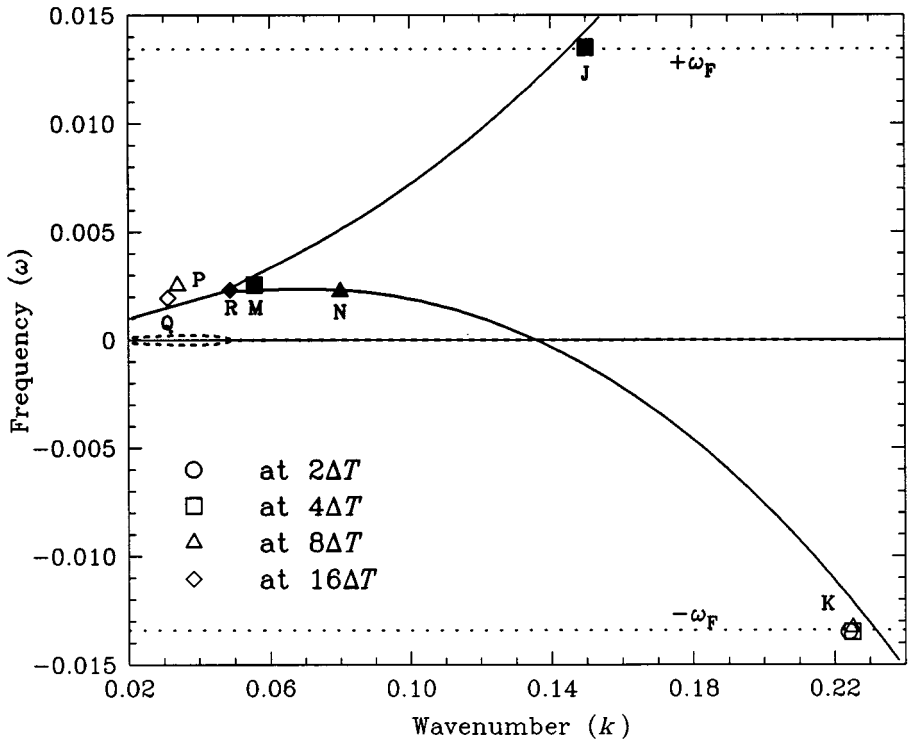

Figure 13. Locations of waves seen in figure 8 plotted in the k–ω plane together with the dispersion curve and value of excitation frequency, ω_{F}: open symbols, upstream response; filled symbols, downstream response. Alphabetic labels of data points are referenced in the text.

To appreciate the character of this $(k_{\mathrm{p}}, \omega_{\mathrm{p}}^{*})$-type wave M, an associated numerical experiment has been conducted. The numerical simulation that yielded figure 10 is repeated, except that the driver is now switched off at $t' = 2\Delta T$. At the switch-off time, figure 10*a* has shown that the steady-state modified flexural response is fully established. Thus, in figure 14 a waterfall diagram of the sum of the panel's strain- and kinetic-energy densities is presented for a sequence of times after the driver has been switched off. For clarity, only results for the downstream half of the panel are plotted. At early times, there is evidence of the wall energy of the modified flexural wave (wave J); in the absence of a source of excitation, this wave then dies away. Subsequently, an unstable wave (that is identified in figure 10*b* as wave M) appears. Rays suggesting the propagation of the edges of the wave packet have been sketched; these attempt to highlight the absolute nature of this unstable behaviour. Wave M can therefore be identified with the absolute instability that exists at ω_{p}^{*} as predicted in the analysis of Abrahams & Wickham (1994).

As the unstable wave M elucidated by the 'switch-off' numerical experiment amplifies, wall energy is carried to the trailing edge of the panel. Thus the next stage of response, represented by figure 10*c*, sees the development of a shorter wavelength disturbance (wave N) near the trailing edge. Identified in the (k, ω)-plane of figure 13, it lies slightly to the right of the maximum of the lower branch. Moreover, we are able to show that it possesses exactly the same character as the type II wave which appeared in figure 3*b* (and in figure 6) at the trailing edge in the simulations for low-

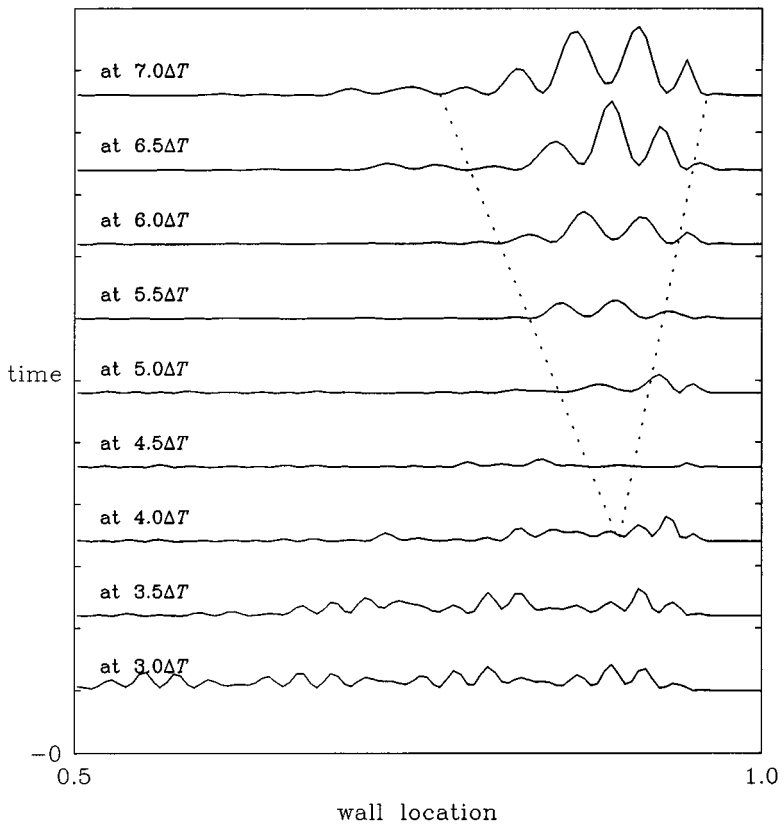

Figure 14. Evolution of total wall energy density for waves found downstream of the driver in figure 10*a*, *b*. In this simulation the driver has been switched off at $t' = 3\Delta T$, otherwise the parameters are identical to those of figure 10.

frequency excitation. It thus convects wall energy in the upstream direction, albeit very slowly; its mean wall energy density propagation speed is approximately equal to the magnitude of the group velocity predicted at the appropriate wavenumber in figure 2*b*. Upstream of the driver, a new longer wavelength disturbance (wave P) is seen to be developing. The energy record, figure 12*a*, shows a change from neutral stability to instability at approximately $11\Delta T$. This can be associated with the generation by the leading edge of wave P, which has the properties of a type I wave (downstream-travelling, spatially growing and with wall energy density propagating in the downstream direction). Numerical experiments with a longer panel show that both the upstream and downstream developments found here at $t' = 8\Delta T$ occur at later times. However, the wavenumbers and frequencies of the emerging waves are the same as for the basic configuration.

Thereafter, the path to continued growth qualitatively follows that described above for low-frequency excitation. For example, figure 10*d*, at $t' = 16\Delta T$, displays type I unstable waves (waves Q and R) both upstream and downstream of the driver. Wave conversions between type II (upstream propagation of wall-energy density) and type I (downstream propagation of wall-energy density) waves are not as clearly identifiable in, for example, the energy plot of figure 12*b* as they were in the equivalent

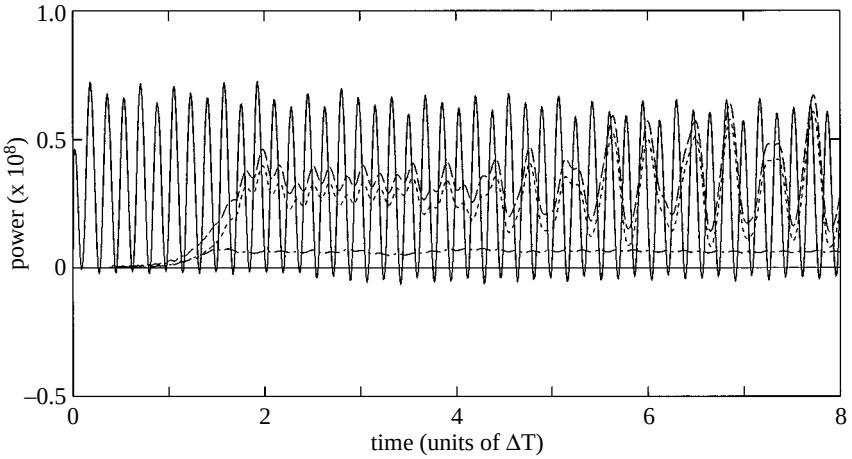

Figure 15. Records of driver power and energy-dissipation rate at the panel ends for high-frequency excitation: ——, driver power; – – –, total dissipation rate at panel ends; – · – · –, dissipation rate at upstream end; - - - -, dissipation rate at downstream end.

low-frequency excitation plot of figure 4*b*. This is because the two classes of waves involved in the present experiment have lower-branch wavenumbers on the dispersion curve that straddle k_{p} more closely. However, it does appear, once again, that repeated wavenumber conversions at the panel ends establish a mechanism that is able to distribute the wall energy to all parts of the panel. In the case of high-frequency excitation used here, this mechanism prevails despite the initial presence and growth of a wave that is best described as an absolute instability. The importance of the absolute instability lies in its acting as an effective initiator for low-frequency convectively unstable disturbances.

Finally, a plot of driver power and rate of energy dissipation close to the panel ends is shown in figure 15. In contrast to the low-frequency excitation, it can be seen that, as predicted by Crighton & Oswell (1991), the mean driver power is positive with the initial steady state reached at $t' = 2\Delta T$. Following this time, the dissipation rate balances that of the driver input. This continues despite the fact that instability sets in downstream of the driver at about $t' = 4\Delta T$. This provides further evidence that the initial instability in the time range t':$4\Delta T \rightarrow 8\Delta T$ is absolute in character; an instability convecting wall-energy density in the downstream direction would have produced a dramatic rise in dissipation at the downstream end similar to that seen in figure 8.

(*b*) *Three-dimensional simulations*

The two-dimensional simulations of the flexible-wall–flow interaction suggest that driving the panel at a prescribed frequency cannot prevent the eventual formation of instability. This might be expected for the low-frequency excitation in which analytical studies also predict unstable waves. However, it has also been shown that while high-frequency excitation first yields a steady-state neutrally stable response (as seen in figure 10*a*), this breaks down to give instability. From the hydroelastician's point of view, it is reasonable to question whether this is an artifice attributable to the assumption of a panel of infinite span. Thus, we briefly present here the more realis-

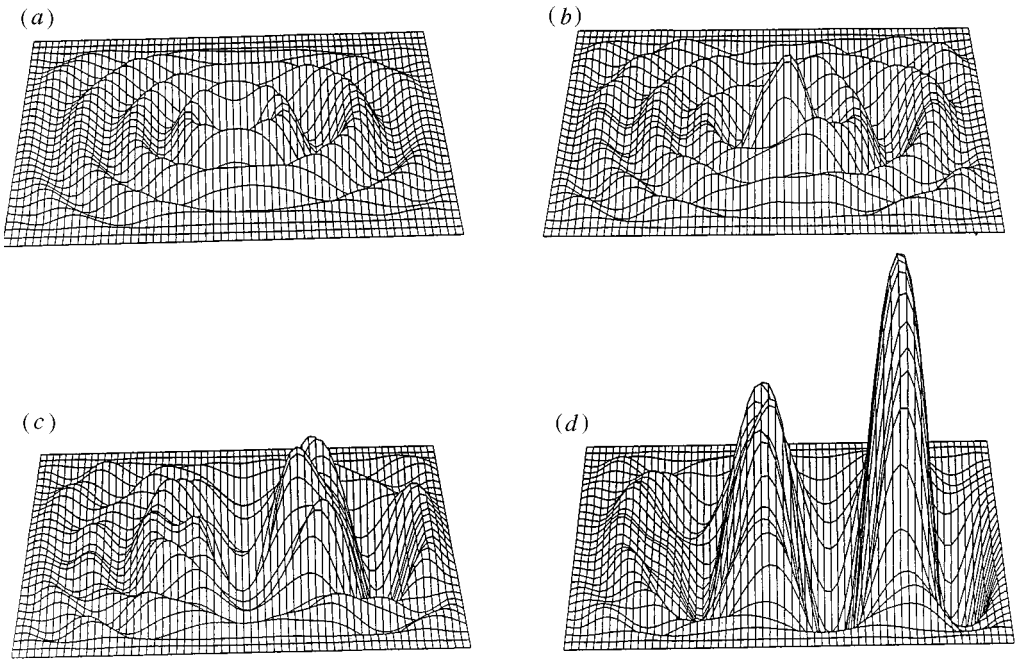

Figure 16. Three-dimensional numerical experiment for high-frequency excitation, $\omega_{\mathrm{F}} = 0.01343$ and flow speed $U' = 0.05$; a point excitation is located at the centre of the panel. Fluid flow is from left to right. Snapshots of panel response at different times: (*a*) $t' = 0.5\Delta T$; (*b*) $t' = 1\Delta T$; (*c*) $t' = 1.5\Delta T$; (*d*) $t' = 2\Delta T$.

tic case of a truly finite panel supporting three-dimensional disturbances undergoing excitation by an oscillatory point driver.

The methods described in § 2 are equally applicable to the three-dimensional problem. The wall stiffness term is replaced by the biharmonic operator and the boundary elements used in the flow solution now become panels. The algorithm used for the system solution is a slightly modified version of that presented in Lucey & Carpenter (1992*b*). A 64×64 SIMD machine was used for the computations. A panel of dimensions $0.3L \times 0.3L$ is used. It has hinged edges on all four sides and, again, damping has been included in the region adjacent to these edges. The remaining data are identical to those used in the two-dimensional work.

Figure 16*a–d* illustrates the response of the panel to high-frequency excitation, $\omega'_{\mathrm{F}} = 0.01343$, at $U' = 0.05$. The flow is from left to right and panel deflections have been scaled up by a factor of 30 000. The plots are for successive increments of time $0.5\Delta T$ after start-up. Thus the experiment is equivalent to the second group of two-dimensional simulations described in § 3 (*a*) except that here we use point excitation; the two-dimensional experiments are driven by line excitation. This choice of driver predisposes the panel to three-dimensional waves and, accordingly, more closely models the situation that is likely to be seen in any real application.

The results indicate that the two-dimensional simulations give a good approximation to the long-term response evolution. At early times, three-dimensional modified flexural waves radiate out from the driver. The difference in upstream and downstream propagating waves is not great but is identifiable in figure 16*a*; for a midspan

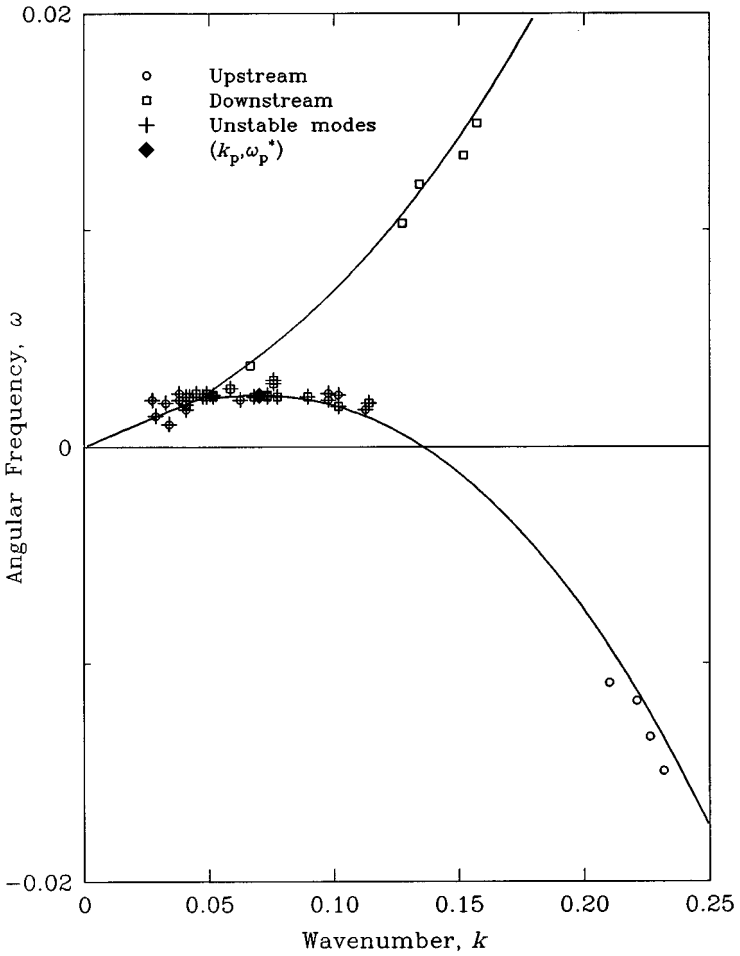

Figure 17. Summary of waves found in a series of numerical experiments plotted as discrete $(k, \mathrm{Re}(\omega))$-data together with the dispersion curve.

cross-section, these exactly match the two-dimensional results seen in figure 10*a*. At later times, the evolution of quasi-two-dimensional unstable waves is apparent. These take the form of downstream-travelling waves although, as evidenced by figure 16*d*, the instability eventually spreads throughout the panel. In fact, the instability mechanism appears to be very similar to that found in the two-dimensional work. In figure 16*d*, the wave seen downstream of the driver possesses the same wavenumber as its counterpart generated at the trailing edge in figure 10*c*. That it should appear earlier in the three-dimensional work is a consequence of using a panel of shorter length and, in some measure, the additional restraints provided by the side edges.

The three-dimensional work thus confirms that the instabilities of the wall–flow system can be modelled as plane waves even when the source of excitation predisposes the disturbances to transverse variations. Furthermore, the sequence of events that leads to the overall destabilization in the two-dimensional work is again found when a truly finite panel is studied.

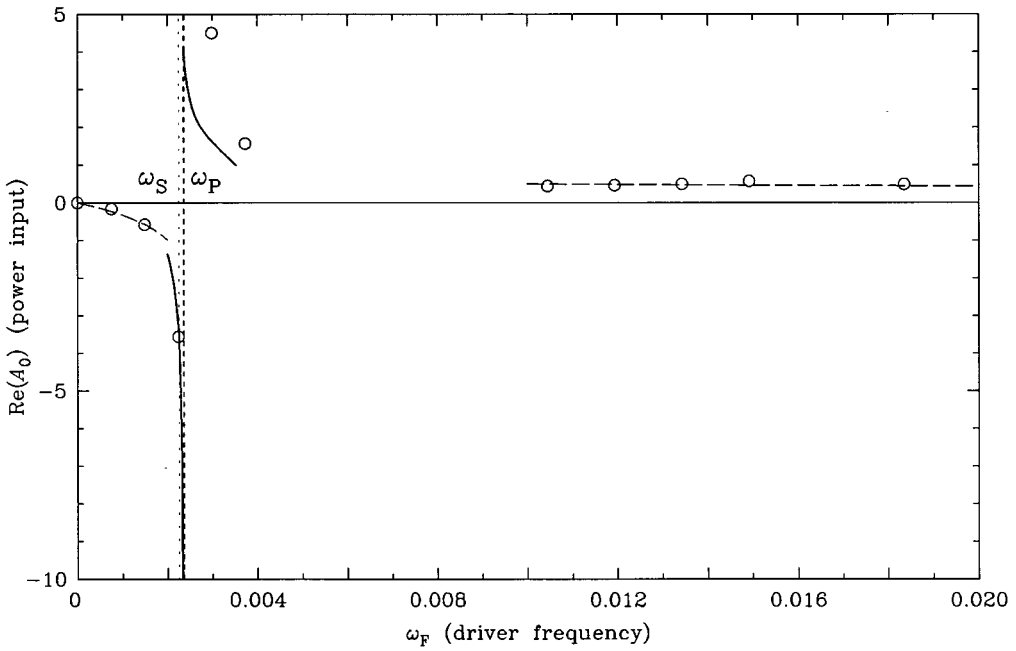

Figure 18. Variation of mean driver power with excitation frequency; comparison of present results with those of Crighton & Oswell (1991): ○, present work; ——, exact solutions from Crighton & Oswell (1991); – – –, asymptotic solutions from Crighton & Oswell (1991).

4. Discussion

Results from just two of the two-dimensional numerical experiments were presented in § 3. However, the present investigation has encompassed a wide range of excitation frequencies. To provide an overall appreciation of the waves, $(k, \mathrm{Re}(\omega))$, that may be found in such simulations, figure 17 plots the location of each against the background of the dispersion curve appropriate to an undamped infinitely long flexible plate. Data scatter might be expected at both high and low wavenumbers, the former reflecting an increasing lack of resolution in the discretization of the numerical scheme and the latter because the ratio of wavelength to panel length is high enough to over-constrain the wave. The data plotted are for an approximately equal number of high-frequency excitations ($\omega_\mathrm{F} > \omega_\mathrm{p}$) and low-frequency excitations ($0 < \omega_\mathrm{F} < \omega_\mathrm{p}$). It is interesting to note the concentration of disturbances in the wavenumber range, $0.03 < k < 0.12$ and the frequency band close to ω_p. For the panel being studied, this figure (like figures 5 and 13) shows that waves in this domain may appear both upstream and downstream of the driver location.

A second summary plot, figure 18, shows the mean driver power against the excitation frequency. The data for this figure have been obtained by time-averaging the driver power from results such as those presented in figures 8 and 15. The time averages have been taken over periods after the evident start-up procedure and before strong end-effects come to dominate the response of the entire panel. The present results show excellent agreement with the predictions of Crighton & Oswell (1991). It may therefore be surmised that the present near-field response matches that predicted by Crighton & Oswell. In the present context, a possible explanation for the

driver absorbing energy for responses below ω_p^* is that the hydroelastic instability found throughout this frequency range converts mean fluid kinetic energy into flexible-plate energy and thereby effectively drives the line excitation. For an infinite flexible plate it has been noted that damping promotes instability (see figure 2*b*) for the lower-branch range of wavenumbers associated with $0 < \mathrm{Re}(\omega) < \omega_p^*$; in an analogous sense, then, the realization of instability is accompanied by energy removal from the flexible plate.

It is in the far-field response that certain differences appear between the present work and that of Crighton & Oswell (1991), even at times before wave conversions at the leading and trailing edges take effect. In the following, we will use Crighton & Oswell's wavenumber notation. In the frequency range, $\omega < \omega_s$, Crighton & Oswell predict a k_1^+, k_2^+ convectively unstable wave downstream of the driver. Our results find a spatially growing wave here that we have shown to propagate wall energy density in the downstream direction; we have termed this a type I wave. However, in the simulations, its frequency does not necessarily equal that of the driver; instead a wave of this type seems to be selected by amplification rate. Upstream of the driver, Crighton & Oswell predict two neutrally stable waves. One of these, denoted k_3^-, is a conventional upstream-travelling wave associated with the lower branch of the dispersion curve for $\mathrm{Re}(\omega) < 0$; it propagates energy away from the driver. A corresponding wave is found in our simulations. The second, denoted k_3^+, is a neutrally stable downstream-travelling negative-energy wave with negative (upstream-directed) group velocity but energy flux directed downstream. This wave then carries energy towards the driver. The numerical simulations find a similar wave associated with the lower branch of the dispersion curve where $k_p < k < k_c$. However, we find it to be unstable, albeit with a very small growth rate. This type of wave can also appear downstream of the driver when the trailing edge is effectively acting as a wave source; under these circumstances it may be considered as being located upstream of its point of initiation. We have termed this a type II wave. When it originates at the trailing edge, we have shown (see figure 7) that it propagates wall energy density in the upstream direction. We can also show that this form of wall energy density propagation occurs when its source is the driver. The absence of flexible-plate damping in Crighton & Oswell (1991) may explain the difference in the stability character of this k_3^+ wave. The analysis of Atkins (1982) of a damped infinitely long flexible plate showed this wave to be unstable and this is consistent with its classification by Crighton & Oswell (1991) as a negative-energy wave. In contrast, the present work clearly shows that damping is not an essential ingredient of the instability mechanism of the equivalent wave on a *finite* flexible panel. Furthermore, the overall indifference of this unstable wave to damping suggests that it does not behave like a negative-energy wave. Rather, it suggests that, on a finite panel, there is a closer association with a class C unstable wave in the Benjamin/Landahl classification (similar to a Kelvin–Helmholtz instability). In associating it with a class C instability, we are then able to use the group velocity obtaining from a dispersion diagram to signify the propagation direction of wall energy density and to approximate the speed of propagation.

In the frequency range, $\omega_s < \omega < \omega_p$, waves found upstream of the driver possess the same character as those described in the previous paragraph. Accordingly, attention is now turned to waves found downstream of the driver for this frequency range. In the subrange $\omega_s < \omega < \omega_b$, two neutrally stable downstream-travelling

PHILOSOPHICAL TRANSACTIONS OF THE ROYAL SOCIETY A MATHEMATICAL, PHYSICAL & ENGINEERING SCIENCES

waves are predicted by Crighton & Oswell (1991). The first is a k_2^+ wave which has a (negative) group velocity directed towards the driver. This violates the usual radiation condition of outward group velocity and so has led to its being described as 'anomalous' by Crighton & Oswell. However, they also show that it is a negative-energy wave and this feature, in combination with its group velocity, means that it has downstream-directed energy flux. Thus, Crighton & Oswell show that, in energy terms, the wave possesses conventional behaviour because it carries energy away from the driver. The second is a k_1^+-type wave. This has a (positive) group velocity directed outwards from the driver and so is conventional in terms of the standard radiation condition. However, this wave is shown to be unusual in energy terms; its energy flux must be directed towards the driver because it also is a negative-energy wave. The second subrange in Crighton & Oswell's analysis has $\omega_b < \omega < \omega_p$. In this range the k_1^+ wave, discussed immediately above, is also found. Additionally, a neutrally stable k_2^+ wave appears with (positive) downstream-directed group velocity and downstream-directed energy flux; this is a positive-energy wave and lies on the upper branch of the dispersion curve. In contrast, all of the other waves predicted downstream of the driver in the frequency range $\omega_s < \omega < \omega_p$ lie on the lower branch of the dispersion curve. In the numerical experiments we are unable to find evidence of any of these waves. In fact, the behaviour throughout the frequency range $\omega < \omega_p$ is characterized by spatially growing waves which propagate wall energy density in the downstream direction and are most closely allied with Crighton & Oswell's k_1^+, k_2^+ unstable wave. In the present work we have termed these type I waves. In the numerical simulations, it may be that the frequency range $\omega_b < \omega < \omega_p$ is simply too narrow to isolate the unusual k_2^+ and k_1^+ waves predicted by Crighton & Oswell. If so, then this may be the case in a physical experiment. However, it could be that the present study of a fluid-loaded *finite* panel represents a distinct system that precludes comparison with one based upon the assumption of an infinitely long flexible plate. This possibility is explored below.

The present work has sought to determine the evolution and characteristics of the waves leading to the overall increase of flexible-plate energy that signifies destabilization of the panel. Within this context, numerical experiments have been used to determine the propagation of the wall energy density. We now seek a framework, in the form of a modified dispersion diagram, which can summarize the results of the numerical experiments in terms of wavenumber, wave frequency and propagation of wall energy density. The desired dispersion diagram should characterize the response of a finite panel and thereby represent a continuous assembly of all the waves found and plotted as discrete data in figures 5 and 13, together with the results of other numerical experiments. Lucey & Carpenter (1993*a*) suggested that the condition of finiteness has an effect which appears to be similar to that of damping in an infinitely long flexible-wall–flow system. Also, Abrahams & Wickham (1994) found that damping exercises a significant effect in the infinite driven-wall system. In figure 19, a dispersion curve for the infinite system has been evaluated for the case of a damped flexible plate. The value of the non-dimensional damping coefficient used is high; it is the same as the maximum value in the range of coefficients of distributed damping investigated and discussed in § 3. We remark that, at early times, the results of numerical experiments with this value of distributed damping showed little difference from those of a panel which had no distributed damping in the main part (the central 90% of panel length). Even at later times, the qualitative pattern

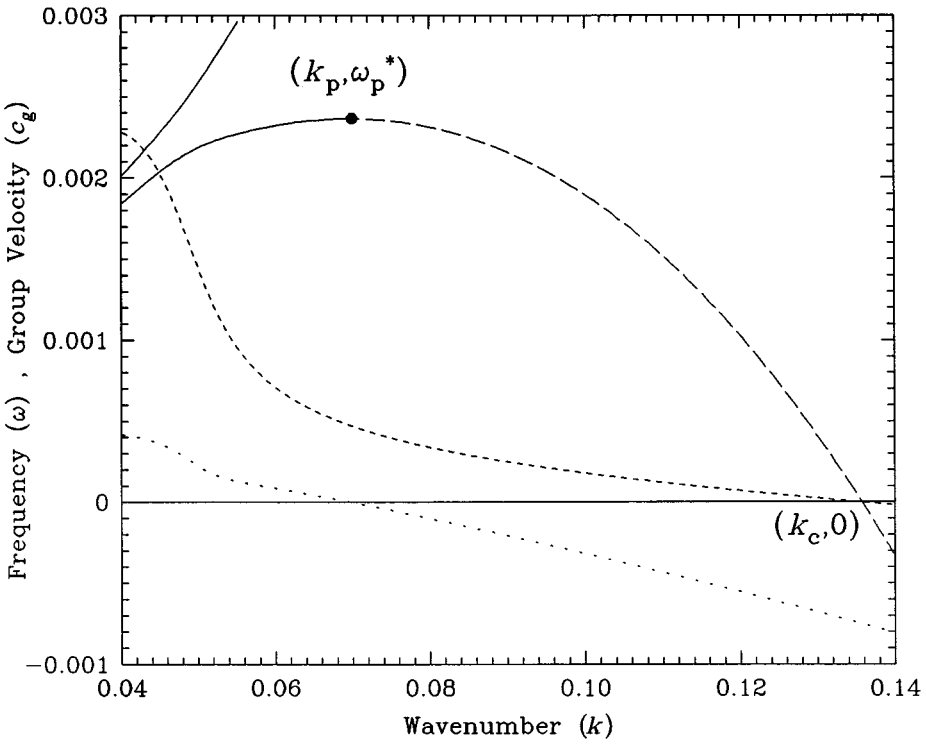

Figure 19. Dispersion diagram and group velocity, c_g, for an infinite flexible panel with plate damping. Temporal description of wave development ($\omega = \omega_R + i\omega_I$): ——, ω_R downstream; – – –, ω_R upstream; - - - -, $\omega_I \times 10$ lower branch; · · · ·, $c_g \times 0.01$, lower branch.

of wave behaviour in the panel-edge interactions remained unchanged. In figure 19, the assumption of temporal instability is made. The key feature of this figure, when compared with the zero-damping case of figure 2*a*, is the change in structure close to the point of modal coalescence. With distributed damping there is no longer *exact* coupling between lower and upper branches and the convective instability associated with the k_1^+, k_2^+-type wave pair blends into the divergence type of instability associated with the higher wavenumbers and $\mathrm{Re}(\omega) > 0$ of the lower branch.

The system response predicted by figure 19 is far simpler and seems a closer representation of the findings from the present numerical experiments for a finite panel. This is not to imply that damping and finiteness are equivalent; rather, it seems that one effect of damping in an infinitely long flexible-plate–wall system is to reproduce approximately a key effect of finiteness. Thus, at low wavenumbers in figure 19, coalescence instability of the k_1^+, k_2^+ type is seen. Increasing the wavenumber gradually decouples these into a damped upper-branch k_2^+-type wave and an unstable lower-branch k_1^+-type wave. On the lower branch, a further rise in wavenumber sees the k_1^+-type wave reach the point (k_p, ω_p^*) at which coalescence with the k_3^+-type wave occurs. This yields an absolute instability at ω_p^*. For wavenumbers in the range $k_p < k < k_c$, the lower-branch wave is of k_3^+ type and weakly unstable. For $k > k_c$, damped upstream-travelling modified flexural waves of the k_3^- type are predicted. In this model, then, the only clearly significant point on the lower branch is (k_p, ω_p^*). Waves in the wavenumber region $0 < k < k_p$ are predicted to be strongly unstable

and to have positive group velocity. The features described above characterize the type I waves found in the numerical experiments when the group velocity implied by figure 19 is associated with the propagation of wall energy density. In contrast, waves in the region $k_{\mathrm{p}} < k < k_{\mathrm{c}}$ are predicted to be weakly unstable and have negative group velocity. Similar characteristics are displayed by the type II waves found in the numerical experiments; such waves have been shown to propagate wall energy density in the upstream direction. Again, the group velocity from this dispersion model is to be interpreted as a prediction of the propagation velocity of wall energy density. The dispersion model of figure 19 thus appears to provide a good description of the waves and wall energy fluxes that predominate on an essentially undamped finite panel for wavenumbers where there is strong flexible-wall–flow coupling. The structure of the dispersion curve of figure 19 renders unlikely any difference in wave classification between the modal-coalescence instability and the lower-branch (i.e. divergence-type) instabilities. This gradual merging of instability types as opposed to explosive coupling was also found by Lucey & Carpenter (1992*a*) in the hydroelastic study of a finite compliant wall.

From the numerical experiments, it therefore appears that the inclusion of sufficient damping in the analysis of an infinitely long wall–flow system can lead to predicted behaviour that is more similar to that found for finite panels with fixed ends. The analysis of Abrahams & Wickham (1994) included plate damping and all frequencies which would be generated in the start-up procedure. They found that the system response was ultimately dominated by an absolute instability at $(k_{\mathrm{p}}, \omega_{\mathrm{p}}^{*})$. It is noteworthy that the time-scales upon which this instability grows are long. Only with a substantial passage of time would the absolute instability come to dominate the response. Thus, the detailed predictions of Crighton & Oswell (1991) would hold before this time and after the start-up transients have convected away. The present investigation of a finite panel also features an absolute instability close to $(k_{\mathrm{p}}, \omega_{\mathrm{p}}^{*})$ at early times and so shows agreement with Abrahams & Wickham (1994). However, at later times we show that the panel's unstable behaviour is dominated by spatially-growing waves which are then repeatedly excited by the panel ends. The effective growth rate of the whole flexible panel arising from this mechanism outweighs that of the absolute instability. Here, the absolute instability has been shown to be important only for high-frequency excitations as a precursor to the spatially growing type I and type II waves, whereas for low frequencies these instabilities are initiated immediately after start-up.

Given that the present investigation highlights the importance of the convective growth of disturbances throughout the range of wavenumbers for which the lower-branch waves have positive phase speeds, the dispersion curve of figure 19 is, perhaps, inappropriate. Accordingly, figure 20, shows a similar model of dispersion devised to predict the waves on a finite panel but based upon the assumption of convective instability. All disturbances are assumed to be proportional to $\exp[\mathrm{i}(kx - \omega t)]$ with $k = k_{\mathrm{R}} + \mathrm{i}k_{\mathrm{I}}$; negative k_{I} indicates instability for increasing x. The principal features of figure 19, discussed above, are equivalently reproduced. It is found that k_{I} is positive for the downstream-travelling wave found upstream of the driver. In the direction of phase velocity this might, at first sight, suggest an attenuating wave thus contradicting the prediction of instability by the temporal approach. However, this wave has negative group velocity. If the group velocity is used to signify the direction of wall energy density transmission, it is propagating in the upstream direction and so

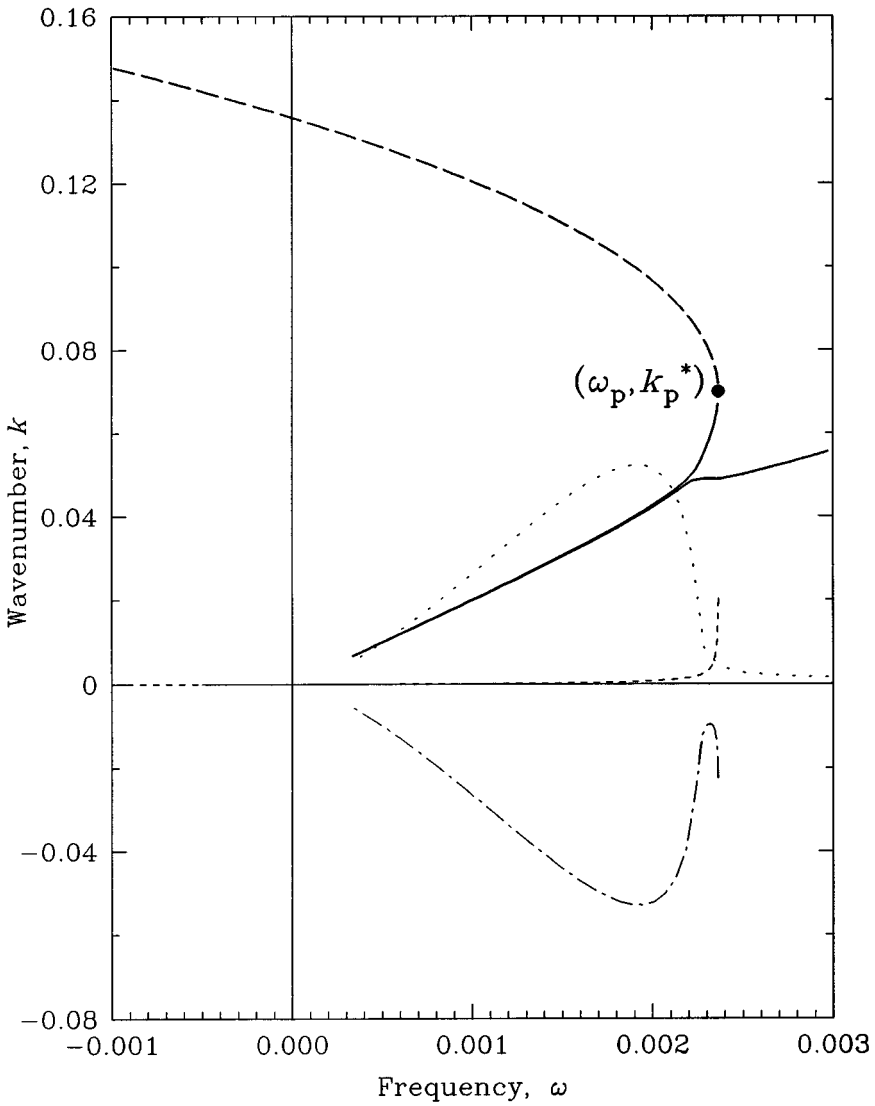

Figure 20. Dispersion diagram for an infinite flexible panel with plate damping. Spatial description of wave development ($k = k_R + ik_I$): ——, k_R, downstream; – – –, k_R, upstream; – · – · –, $k_I \times 10$, lower left branch; - - - -, $k_I \times 10$, upper left branch; · · · ·, $k_I \times 10$, right branch.

$+k_I$ would represent the growth rate. In the numerical experiments this corresponds to a type II wave which convects wall energy density in the upstream direction and slowly amplifies as it does so. It is noted that singular behaviour occurs at (ω_p, k_p^*) in the solution of the proposed dispersion model. This is seen in the imaginary parts of the wavenumber and it suggests the coalescence of convective waves at k_p^*. Abrahams & Wickham (1994) also noted that the inclusion of damping fundamentally changed the morphology of the complex k-plane thereby generating an absolute instability. Such behaviour might be qualitatively anticipated; as ω_p is approached, the group velocity tends to zero and thus any convective representation of instability must

have growth rates tending to infinity. A better approximate approach to modelling the instability exactly at (ω_p, k_p) is to adopt the temporal assumption (as used in generating figure 19).

In the proposed dispersion models of figures 19 and 20, we have located waves as existing either upstream or downstream. This description is applied relative to the driver at early times of the numerical simulations. Following the principles laid down by Crighton (1994), we similarly note that, at later times, the panel ends act as sources for waves. For example a type II wave is excited by the trailing edge; it thus appears in an *upstream* location and the notation used in the dispersion diagram remains consistent. So, too, a type I wave is excited at the leading edge; it then appears in a *downstream* location relative to its source of excitation.

Experimental studies of hydroelastic instability tend to focus on the flow speed at which instability first appears. The study of an infinitely long flexible plate with some damping (Abrahams & Wickham 1994) suggests that in the long-time limit this flow speed would be zero due to the absolute instability at (k_p, ω_p^*). In contrast, experimental studies necessarily use a finite panel and the structure of the flexible wall is such that more than one structural effect contributes to the overall interfacial restorative force. Gad-el-Hak *et al*. (1984) and Hansen & Hunsten (1983) used a viscolelastic slab as the flexible wall; in this case, a combination of the material elastic modulus and its depth determines the effective restorative force. In Djugundi *et al*. (1963) a flexible plate resting on a spring foundation constituted the flexible wall; in this case, the combination of plate bending stiffness and spring stiffness provides the overall restorative force. The more complex flexible wall modelled by Dixon *et al*. (1994), based upon the structure of the compliant wall used in the experiments of Gaster (1987), comprised a flexible plate adhered to a viscoelastic substrate. In this case, the restorative force comprised contributions from the plate bending stiffness, the substrate elastic modulus and the thickness of the substrate. For all of these types of multicomponent flexible walls, a non-zero critical speed is found. This critical speed is determined by the combination of flow and structural parameters. The first instability encountered, which is attributable primarily to potential-flow effects, has often been termed static divergence (see, for example, Gad-el-Hak *et al*. 1984; Hansen & Hunsten 1983). The instability appears as a very slow (almost static) downstream-travelling wave. It also has the character of an absolute instability because growth is seen at all spatial locations of the compliant wall. The identification of (k_p, ω_p^*) as a point of absolute instability in the present investigation and that of Abrahams & Wickham (1994) is consistent with the experiments. For a compliant wall with more than one structural parameter, theoretical predictions of divergence instability have it first appearing when the maximum on the lower branch of the dispersion curve first crosses the k-axis with increasing flow speed. Exactly at the critical speed, this maximum lies on the $\omega = 0$ axis yielding a static wall deformation. An example of this type of critical situation is seen in figure 4 of Dixon *et al*. (1994). Just above the critical flow speed, a small loop of the the lower branch lies in the upper half of the frequency plane and so the maximum takes a very low positive value of ω. Thus, a wave is predicted at the maximum which has a very low positive phase speed and which is absolutely unstable because it is now represented by the (k_p, ω_p^*)-point of the lower branch of the dispersion curve. These predictions qualitatively agree with the realization of divergence instability in experimental work. A further rise in the applied flow speed sees what experimentalists (see, for example, Dugundji *et al*.

1963) describe as flutter instability replacing the divergence. In such a regime, theoretical predictions then suggest that a range of waves may be unstable; these can be identified with the downstream-travelling part of the lower branch of the dispersion curve which moves into the upper k-plane. The flow speed used in the generation of figures 19 and 20 is representative of this situation. Thus, spatially growing waves can now coexist with an absolute instability modified by the higher flow speed to have a higher phase speed. The present work then suggests that ultimately these spatially growing, or flutter-type, waves would characterize the overall destabilization process of a panel at post-critical (divergence-onset) flow speeds.

5. Conclusion

The method of numerical simulation has been used to conduct an investigation of the response of a finite flexible panel to oscillatory line excitation when a mean flow is present. A series of numerical experiments has been carried out in order to identify the different waves that might exist on the panel and to compare these, where appropriate, with the predictions of theoretical studies based on the assumption of an infinitely long flexible plate. The present study finds the overall response of the panel to be unstable even at very low flow speeds and that finiteness plays an important part in the detailed mechanism responsible for the unstable behaviour. This is because the present method allows frequencies different from that of the driver to enter the response; these other frequencies may be generated either in the start-up process or by energy scattering at the panel's ends. However, at early times, qualitative agreement is found with the theoretical studies of an infinitely long plate.

Prior to strong interactions at the panel's leading and trailing edges, the response of the panel can be grouped into two different types: low- and high-frequency excitation. The frequency that divides these two groups is ω_{p}. This is the frequency at the maximum of the lower branch in the (k, ω) dispersion diagram. Low-frequency excitations can be characterized by a downstream-travelling spatially growing wave found downstream of the driver; this has been shown to convect wall energy density in the downstream direction. This corresponds to the k_1^+, k_2^+ convectively unstable wave of Crighton & Oswell (1991). Upstream of the driver, two waves are found. One corresponds to a conventional upstream-travelling modified flexural wave denoted k_3^- by Crighton & Oswell. The other is downstream-travelling and marginally unstable. A wave with similar features, also found in the numerical simulations but emanating from the trailing edge, is shown to propagate wall energy density in the upstream direction. This response corresponds most closely to the k_3^+ negative-energy wave of Crighton & Oswell. However, on a finite panel, the unstable character of the wave is not dependent upon wall damping. A subtle difference, warranting further investigation, may exist between the present finite-panel system and the Crighton & Oswell study of an infinitely long flexible plate. In the present work, the two spatially growing instabilities act to transmit wall energy to the panel edges. The wave downstream of the driver has a much higher growth rate and would be the most dominant feature in a physical experiment. High-frequency excitations also feature a propagation of wall energy density to the leading and trailing edges by an unstable wave. In this case the first response is one of modified flexural waves radiating out from the driver. After an initial steady state is achieved, breakdown occurs through the growth of an absolute instability. Abrahams & Wickham (1994) predicted the existence of absolute insta-

bility for a damped infinitely long flexible plate. In the present finite-panel work, the corresponding instability is not dependent upon the inclusion of panel damping. The amplitude growth associated with this instability spreads sufficient wall energy to the leading and trailing edges so that strong end effects come into play. In the present work it has proved impossible to find the unusual waves predicted by Crighton & Oswell (1991) in the frequency range $\omega_s < \omega < \omega_p$. This could be because the present numerical simulation is too coarse a tool to isolate the responses in this narrow frequency band or because the finite panel does not necessarily respond at the driver frequency. In the present numerical simulations, unstable waves at frequencies other than that of the driver may be preferentially excited on the basis of amplification rate. On an infinitely long flexible plate with single-frequency continuous excitation these would be convected away downstream.

At later times, both low- and high-frequency responses show the same qualitative pattern of behaviour. Wave conversions at the panel ends generate a succession of spatially growing waves which are capable of propagating wall energy density both in the downstream and upstream directions. For example, an unstable wave propagating wall energy density downstream may first grow. As it reaches the final extent of its growth, limited by the panel's finite length, it excites a different unstable wave which propagates wall energy density in the upstream direction. At its initiation, the amplitude of this new wave effectively matches that of its precursor. The spatial growth of this wave in the upstream direction is halted by the leading edge. At the leading edge, it then excites a spatially growing wave propagating wall energy density in the downstream direction and the destabilization sequence repeats itself once more. Both the line excitation and the panel ends can act as energy scatterers for wave initiation, although for larger amplitudes the driver becomes increasingly ineffective. In fact, any strong local inhomogeneity in the panel, such as a patch of high stiffness, can act as an energy scatterer.

A dispersion diagram for the waves found on a finite panel has been artificially generated by modifying the dispersion relation for an infinitely long flexible panel through the inclusion of substantial flexible-plate damping. The structure of the resulting diagram appears to represent closely the findings of the present numerical experiments. The pair of spatially growing waves that dominate the long-time unstable behaviour of the panel, termed type I and type II waves in the present work, are identified on this dispersion diagram as straddling the point (k_p, ω_p^*) where absolutely unstable behaviour exists. The direction and mean speed of propagation of wall energy density effected by the type I and type II waves are predicted by the group velocity associated with this dispersion diagram.

A particular feature of the present finite system is that spatially growing waves can organize themselves so that all locations of the panel experience disturbance growth. For an infinite system, only an absolute instability could achieve this. Furthermore, in the present work, this convective mechanism dominates the response despite the presence of an absolute instability. Thus, in the destabilization process, an experimentalist could expect to see a succession of downstream-travelling waves and continuous amplitude growth. Careful observation would identify different dominant wave types at successive times in the evolution: a type I longer-wavelength disturbance with rapid growth and higher phase speed alternating with a type II shorter wavelength disturbance spreading from the trailing edge and having a lower phase speed and much slower growth. The time period between these alternating modes of

response would be determined by the panel's length. This sequence of events could be expected to continue to yield amplitude growth until nonlinear effects became important.

The sequence of hydroelastic events described above might also be modified if a boundary layer were to be included in the flexible-wall–flow model. The modified flexural wave typified by the upper branch of the dispersion curve in figure 2 is prone to travelling-wave flutter when irreversible energy exchanges are made possible by the action of a boundary layer. This convective instability may be significant given the apparent predominance of convective wall energy mechanisms in the present system. This feature of a real flexible-wall–flow interaction requires further study along with nonlinear effects. Lastly, it is remarked that the wall model used in the present investigation is particularly vulnerable to hydroelastic instability. Comprising only a flexible plate, its critical (divergence-onset) flow speed approaches zero as the panel length is increased. Attempts to control hydroelastic instability using line excitation will manifestly fail given the present results. A more practical problem might be to investigate whether a flexible wall comprising a combination of restorative elements is amenable to control.

The author thanks Professor P. W. Carpenter (University of Warwick) and Professor I. D. Abrahams (University of Manchester) for their valuable suggestions during discussions of this work. The author also thanks Professor D. G. Crighton (University of Cambridge) for his many useful comments on the work.

References

Abrahams, I. D. & Wickham, G. R. 1994 Lecture at EUROMECH Colloq. 316, Manchester.

Akhieser, A. I. & Polovin, R. V. 1971 Criteria for wave growth. *Sov. Phys. Usp.* **14**, 278–285.

Atkins, D. J. 1982 The effect of uniform flow on the dynamics and acoustics of force-excited infinite plates. Technical Memo. Admiralty Marine Technology Establishment, Teddington, England, AMTE (N) TM 82087.

Benjamin, T. B. 1960 Effects of a flexible boundary on hydrodynamic stability. *J. Fluid. Mech.* **9**, 513–532.

Benjamin, T. B. 1963 The threefold classification of unstable disturbances in flexible surfaces bounding inviscid flows. *J. Fluid. Mech.* **16**, 436–450.

Brazier-Smith, P. R. & Scott, J. F. 1984 Stability of fluid flow in the presence of a compliant surface. *Wave Motion* **6**, 436–450.

Briggs, R. J. 1964 *Electron-stream interaction with plasmas*. MIT Press.

Cairns, R. A. 1979 The role of negative energy waves in some instabilities of parallel flows. *J. Fluid Mech.* **92**, 1–14.

Carpenter, P. W. 1990 Status of transition delay using compliant walls. In *Viscous drag reduction in boundary layers* (ed. D. M. Bushnell & J. M. Hefner), pp. 79–113. New York: AIAA.

Carpenter, P. W. & Garrad, A. D. 1986 The hydrodynamic stability of flows over Kramer-type compliant surfaces. II. Flow-induced surface instabilities. *J. Fluid Mech.* **170**, 199–232.

Crighton, D. G. 1989 The 1988 Rayleigh medal lecture: fluid-loading—the interaction between sound and vibration. *J. Sound Vib.* **133**, 1–27.

Crighton, D. G. 1994 New aspects of fluid-structure interaction theory. 25th Anniversary Meeting, DCAMM, Technical University of Denmark, pp. 1–16.

Crighton, D. G. & Oswell, J. E. 1991 Fluid loading with mean flow. I. Response of an elastic plate to localized excitation. *Phil. Trans. R. Soc. Lond.* A **335**, 557–592.

Dixon, A. E., Lucey, A. D. & Carpenter, P. W. 1994 The optimization of viscoelastic walls for transition delay. *AIAA Jl* **32**, 256–267.

Dugundji, J., Dowell, E. & Perkin, B. 1963 Subsonic flutter of panels on a continuous elastic foundation. *AIAA Jl* **1**, 1146–1154.

Ellen, C. H. 1973 The stability of simply supported rectangular surfaces in uniform subsonic flow. *Trans. ASME* E **95**, 68–72.

Gad-El-Hak, M., Blackwelder, R. F. & Riley, J. F. 1984 On the interaction of compliant coatings with boundary-layer flows. *J. Fluid Mech.* **140**, 257–280.

Garrad, A. D. & Carpenter, P. W. 1982*a* On the aerodynamic forces involved in the hydroelastic instability of two-dimensional panels in uniform incompressible flow. *J. Sound Vib.* **80**, 437–439.

Garrad, A. D. & Carpenter, P. W. 1982*b* A theoretical investigation of flow-induced instabilities in compliant coatings. *J. Sound Vib.* **84**, 483–500.

Gaster, M. 1968 Growth of disturbances in both space and time. *Phys. Fluids* **11**, 723–727.

Gaster, M. 1987 Is the dolphin a red herring? In *Proc. IUTAM Symp. on Turbulence Management & Relaminarisation, Bangalore, India* (ed. H. W. Liepmann & R. Narasimha), pp. 285–304. Berlin: Springer.

Hess, J. L. & Smith, A. M. O. 1967 Calculation of potential flow about arbitrary bodies. *Prog. Aeronaut. Sci.* **8**, 1–138.

Hansen, R. J. & Hunsten, D. L. 1983 Fluid-property effects on flow-generated waves on a compliant surface. *J. Fluid Mech.* **133**, 161–177.

Huerre, P. & Monkewitz, P. A. 1985 Absolute and convective instabilities in free shear layers. *J. Fluid Mech.* **159**, 151–168.

Huerre, P. & Monkewitz, P. A. 1990 Local and global instabilities in spatially developing flows. *A. Rev. Fluid Mech.* **22**, 473–537.

Kornecki, A. 1978 Aeroelastic instabilities of infinitely long plates. I. *Solid Mech. Arch.* **3**, 281–440.

Kornecki, A., Dowell, E. & O'Brien, J. 1976 On the aeroelastic instability of two-dimensional panels in uniform incompressible flow. *J. Sound Vib.* **47**, 163–178.

Landahl, M. T. 1962 On the stability of a laminar incompressible boundary-layer over a flexible surface. *J. Fluid Mech.* **13**, 609–632.

Lucey, A. D. 1989 Hydroelastic instability of flexible surfaces. PhD thesis, University of Exeter.

Lucey, A. D. & Carpenter, P. W. 1992*a* A numerical simulation of the interaction of a compliant wall and inviscid flow. *J. Fluid Mech.* **234**, 121–146.

Lucey, A. D. & Carpenter, P. W. 1992*b* A study of the hydroelastic stability of a compliant panel using numerical methods. *Int. J. Numer. Methods Heat Fluid Flow.* **2**, 537–553.

Lucey, A. D. & Carpenter, P. W. 1993*a* On the difference between the hydroelastic instability of infinite and very long compliant panels. *J. Sound Vib.* **163**, 176–181.

Lucey, A. D. & Carpenter, P. W. 1993*b* The hydroelastic stability of three-dimensional disturbances of a finite compliant panel. *J. Sound Vib.* **163**, 527–552.

Lucey, A. D. & Carpenter, P. W. 1995 Boundary layer instability over compliant walls: comparison between theory and experiment. *Phys. Fluids* **7**, 2355–2363.

Oswell, J. E. 1992 PhD thesis, University of Cambridge.

Weaver, D. S. & Unny, T. S. 1971 The hydroelastic stability of a flat plate. *Trans. ASME J. Appl. Mech.* E **37**, 823–827.

Yeo, K. S., Khoo, B. C. & Zhao, H. Z. 1996 The absolute instability of boundary-layer flow over viscoelastic walls. *Theor. Comput. Fluid Dynam.* **8**, 237–252.

PHILOSOPHICAL TRANSACTIONS OF THE ROYAL SOCIETY A MATHEMATICAL, PHYSICAL & ENGINEERING SCIENCES

PHILOSOPHICAL TRANSACTIONS OF THE ROYAL SOCIETY A MATHEMATICAL, PHYSICAL & ENGINEERING SCIENCES